TRANSONIC WIND TUNNEL
FOR INVESTIGATION OF TURBOMACHINERY BLADES

Thesis by

Jean-Pierre Dolait

In Partial Fulfillment of the Requirements

For the Degree of

Aeronautical Engineer

California Institute of Technology

Pasadena, California

1971

A Mes Parents

ACKNOWLEDGMENTS

The author wishes to express his most sincere appreciation and thanks to Professor Edward E. Zukoski for his cooperation, guidance, and support throughout this research, and to Professors Toshi Kubota and Frank E. Marble for their continuing interest and invaluable advice.

My grateful appreciation is extended to Messrs. Paul Baloga and George Carlson for their advice, and to Mmes. V. Conner, R. Duffy, and B. Wood for their expert typing of this thesis and the graphs.

I wish to acknowledge the receipt of a teaching assistantship from the California Institute of Technology for the academic year 1970 - 1971.

ABSTRACT

The design of a two-stream wind tunnel was undertaken to allow the simulation and study of certain features of the flow field around the blades of high-speed axial-flow turbomachineries. The mixing of the two parallel streams with designed Mach numbers respectively equal to 1.4 and 0.7 will simulate the transonic Mach number distribution generally obtained along the tips of the first stage blades in large bypass-fan engines.

The GALCIT hypersonic compressor plant will be used as an air supply for the wind tunnel, and consequently the calculations contained in the first chapter are derived from the characteristics and the performance of this plant.

The transonic part of the nozzle is computed by using a method developed by K. O. Friedrichs. This method consists essentially of expanding the coordinates and the characteristics of the flow in power series. The development begins with prescribing, more or less arbitrarily, a Mach number distribution along the centerline of the nozzle. This method has been programmed for an IBM 360 computer to define the wall contour of the nozzle.

A further computation is carried out to correct the contour for boundary layer buildup. This boundary layer analysis included geometry, pressure gradient, and Mach number effects. The subsonic nozzle is calculated (including boundary layer buildup) by using the same computer programs. Finally, the mixing zone downstream of the splitter plate was investigated to prescribe the wall contour correction necessary to ensure a constant-pressure test section.

TABLE OF CONTENTS

LIST OF SYMBOLS

Symbols Introduced in Chapter I

A	half test section area (Chapter I)
a_1	speed of sound for the supersonic stream
a_2	speed of sound for the subsonic stream
$\overline{C_A}$	mean velocity of the gas upstream of the wind tunnel
$\overline{C_B}$	mean velocity of the gas downstream of the wind tunnel
M_1	characteristic Mach number of the supersonic stream
M_2	characteristic Mach number of the subsonic stream
$\dot{M}_1$	mass flow rate of the supersonic stream
$\dot{M}_2$	mass flow rate of the subsonic stream
$\dot{M}$	$= \dot{M}_1 + \dot{M}_2$, total mass flow rate
P_{ot}	total pressure (stagnation condition)
P_s	static pressure
P_{1s}	static pressure of the supersonic stream
P_{2s}	static pressure of the subsonic stream
ΔP_A	pressure drop in the pipes upstream of the wind tunnel
ΔP_B	pressure drop in the pipes downstream of the wind tunnel
$\dot{Q}_i$	volume flow rate at the intake of the compressor plant
$\overline{R_A}$	mean Reynolds number in the pipes upstream of the wind tunnel
$\overline{R_B}$	mean Reynolds number in the pipes downstream of the wind tunnel
T	static temperature
T_i	static temperature at the intake of the compressor plant
T_s	static temperature at the supply of the compressor plant

Symbols Introduced in Chapter I (cont'd.)

V_1	velocity of the supersonic stream in the test section
V_2	velocity of the subsonic stream in the test section
γ	ratio of specific heats, C_p/C_v
λ	compression ratio
ρ_{ot}	mass density at stagnation conditions
ρ_1	designed static mass density of the supersonic stream
ρ_2	designed static mass density of the subsonic stream
ρ_i	static mass density at the inlet of the compressor
ρ_s	static mass density at the supply of the compressor

Symbols Introduced in Chapter II

A	area ratio
A^*	critical area ratio (equals 1)
h	height ratio
$\bar{h}$	centerline height ratio distribution
$\bar{M}$	centerline Mach number distribution
$\bar{u}$	centerline velocity distribution
u^*	critical velocity (at Mach number = 1)
u	velocity x component
v	velocity y component

Symbols Introduced in Chapter III

B	cross section distribution
C_f	shear stress coefficient = $\sqrt{\tau_w/[(\rho_e u^2)/2]}$
C_{fi}	shear stress coefficient after Howarth's transformation
H	integral parameter = δ^*/θ

Symbols Introduced in Chapter III (cont'd.)

H_i integral parameter = δ_i^* / θ_i

K Kármán's constant

Re_δ Reynolds number based on boundary layer thickness = $(\delta \bar{u})/\nu_{ref}$

Re_θ Reynolds number based on momentum thickness = $(\theta \bar{u})/\nu_{ref}$

T_e centerline flow temperature

T_o total temperature (300°K), = T_t

T_{ref} reference temperature (300°K)

T_w wall temperature (300°K)

T_{aw} adiabatic wall temperature (300°K)

$\bar{u}$ centerline velocity distribution

u_τ shear velocity defined as $\sqrt{\tau_w/\rho}$

$u_{i\tau}$ shear velocity after Howarth's transformation

w function describing the boundary layer

y_i y coordinate after Howarth's transformation

δ boundary layer thickness

δ_i boundary layer thickness after Howarth's transformation

δ^* boundary layer displacement thickness

$$= \int_0^\delta \left[1 - \frac{\rho u}{\rho_e \bar{u}} \right] dy$$

δ_i^* boundary layer displacement thickness after Howarth's transformation

θ boundary layer momentum thickness

$$= \int_0^\delta \frac{\rho u}{\rho_e \bar{u}} \left[1 - \frac{u}{\bar{u}} \right] dy$$

Symbols Introduced in Chapter III (cont'd.)

θ_i	boundary layer momentum thickness after Howarth's transformation
$\tilde{\pi}$	function characterizing the boundary layer
ρ_e	centerline flow density
τ_w	shear stress at the wall
ν_o	kinematic viscosity at 300^oK
ν_e	kinematic viscosity of the centerline flow
ν_{ref}	reference kinematic viscosity
μ_e	dynamic viscosity of the centerline flow
μ_{ref}	reference dynamic viscosity

Symbols Introduced in Chapter IV

b	mixing zone thickness
$\bar{b}$	dimensionless parameter characterizing the mixing zone
m	mean stream velocity ratio
$\bar{\rho}$	mean stream density ratio
$\bar{u}_1$	velocity of the subsonic stream outside the mixing zone
$\bar{u}_2$	velocity of the supersonic stream outside the mixing zone
T_1	temperature characterizing the subsonic stream for the mixing zone calculation
T_2	temperature characterizing the supersonic stream for the mixing zone calculation
z	dimensionless parameter characterizing the different profiles of the mixing zone

LIST OF TABLES

LIST OF FIGURES

INTRODUCTION

The use of transonic blades -- whose good efficiency is still not understood -- in high-speed turbomachines has generated new problems in the design of this kind of blade.

If the shank of the blade generally remains subsonic, the tip -- because of the rotational effect -- becomes supersonic, and a complex flow field characterized by a transonic Mach number distribution is created along the length of the blade. To simulate the velocity gradient character of this flow field (note centrifugal effects are not present), a wind tunnel has been designed wherein two parallel flows mix. The two streams (with designed Mach numbers equal to 1.4 and 0.7) will respectively simulate the outer and inner regions of the flow through the turbomachinery. The mixing region of these two streams, in the test section of the wind tunnel, is a good image of the transonic region located at the middle of the blade.

A model blade will be set parallel to the velocity gradient and the pressure field and relaxation of the shock waves will be studied. The study of the interaction of oblique shock waves with the two streams and the constant pressure mixing of the two streams can also be studied with this apparatus.

The different wall contours are computed in the first chapter. A method developed by K. O. Friedrichs is used for the transonic part of the nozzle. The boundary layer correction is developed in Chapter II, and the mixing zone is treated in the last chapter. The general characteristics of the wind tunnel are shown in the Conclusion.

I. CHARACTERISTICS OF THE WIND TUNNEL

1. Flow Rates

The test section (downstream of the splitter plate), where both streams are allowed to mix, is a rectangle of 10 × 5 cm, with each stream occupying a square of 5 × 5 cm. The Mach numbers were chosen to be 1.4 for the supersonic stream and 0.7 for the subsonic stream. Downstream of the splitter, the design requirement is that both streams must have the same static pressure. Given the stagnation conditions upstream of the double nozzle in one stream, we can determine the pressures at different stations and the flow rates (Fig. 1) for both streams. Based on the capabilities of the pumping system, we choose to fix the total pressure in the supersonic stream at one atmosphere.

At Mach number 1.4 we have $P_s = 0.3142\ P_{ot}$, so we get in the test section $P_{1s} = P_{2s} = 0.3142$ atmosphere. But for the subsonic flow at Mach number 0.7 we have $P_s = 0.7209\ P_{ot}$, so it is required to drop the total pressure of the subsonic flow upstream of the nozzle to fit the value of the static pressure in the test section. The new total pressure of the subsonic stream will be:

$$P_{ot} = 0.3142/0.7209 = 0.44 \text{ atmosphere.}$$

This pressure drop will be obtained in the valve controlling the subsonic stream from the value of the static pressure in the test section given by the supersonic stream.

Computation of the flow rate. For the supersonic stream we get

$$\dot{M}_1 = A \cdot \rho_1 \cdot v_1 = A \cdot \rho_1 \cdot M_1 a_1 = A \cdot \rho_1 \cdot M_1 \sqrt{\gamma R T_1} ,$$

and similarly for the subsonic stream; then

$$\dot{M} = \dot{M}_1 + \dot{M}_2 = A\sqrt{\gamma R}\,[\rho_1 M_1 \sqrt{T_1} + \rho_2 M_2 \sqrt{T_2}\,]$$

where subscript 1 refers to the supersonic stream and 2 to the subsonic stream. Given $T_1 = 210^{\circ}K$, $T_2 = 270^{\circ}K$, $R = 2875/kg/^{\circ}K$; $\rho_1 = 0.43\ \rho_{ot}$ and $\rho_2 = 0.34\ \rho_{ot}$, we finally get

$$\dot{M} = 0.77\ kg/s .$$

2. Characteristics of the Compressor Plant

The first and second stages of the GALCIT hypersonic compressor plant will be used for the wind tunnel. This arrangement (see Fig. 2) consists of four Fuller C 300, four Fuller C 300 H, one Fuller C 200, and one Fuller C200 H compressors. The performances of these compressors are described in ref. 1. The characteristic charts 3 and 4 (compression ratio λ as a function of total intake volume flow) will be used to determine the general performance of the whole plant.

3. Characteristics of the Wind Tunnel

Knowing the supply conditions chosen for the tunnel (P_s = 1.1 atmosphere, $T_s = 300^{\circ}K$, $\rho_s = 1.28\ kg/M^3$) and the mass flow rate required by the wind tunnel (0.77 kg/s), we can compute the volume flow rate at the intake as a function of the compression ratio λ.

$$\dot{Q}_i = \frac{\dot{M}}{\rho_i} = \frac{\dot{M}}{\rho_s} \cdot \frac{\rho_s}{\rho_i} , \quad \text{but} \quad T_s \approx T_i , \quad \text{so}$$

$$\dot{Q}_i = \frac{\dot{M}}{\rho_s} \cdot \frac{\rho_s}{\rho_i} = \frac{\dot{M}}{\rho_s} \cdot \lambda .$$

so

$$\dot{Q}_i = 0.6 \cdot \lambda \ m^3/s = 1260 \cdot \lambda \ cf/mn \ .$$

Hence, the characteristic chart of the wind tunnel is a linear function of the compression ratio.

4. Matching of the Two Characteristics (Fig. 5)

When the characteristics are reproduced on the same map, three solutions are found which will give the desired flow. For A, the compression ratio is very small, and a very good recovery factor would be needed in the diffuser. Solutions B and C are very similar; however, C will be considered here because of its better distribution of the power among the ten compressors.

5. Loss in the Pipes

We only can have an approximate value for the loss in the installation; however, we will use, to compute the different pressure drops in the pipes, the following relation:

$$\frac{\Delta P}{\Delta x} = f \frac{\rho \overline{C}^2}{2D}$$

where f is the loss factor and is taken to be 0.03,

$\Delta P/\Delta x$ is the loss per unit length,

ρ is the specific mass of the air,

D is the diameter of the pipe,

$\overline{C}$ is the mean velocity in the pipe.

Given the diameters of the pipes, we can calculate the loss and values are shown in Fig. 6. Two examples were chosen and the results are shown below for the upstream line (A) and the downstream line (B).

For A	For B
for diameter = 6" = 0.15 m	for diameter = 10" = 0.25 m
$\overline{C}_A$ = 36 m/s	$\overline{C}_B$ = 50 m/s
$\overline{R}_A = 4.\,10^6$	$\overline{R}_B = 1.7\ 10^6$
ΔP_A = 0.02 atmosphere	ΔP_B = 0.004 atmosphere

Because the mean velocities considered are relatively small, the loss will be almost negligible. However, we will adopt a pressure drop of 0.1 atmosphere for the upstream pipe and 0.05 atmosphere for the downstream one as a reasonable safety factor when a 10" downstream and 6" upstream diameter pipe are used.

6. Pressure Recovery in the Diffuser

In order to isolate the test section from the diffuser, it was decided to accelerate the flow at the entrance to the diffuser to insure that all the flow outside of boundary layers was supersonic. This requires that the remaining Mach 0.7 flow be accelerated to Mach 1.10. If this flow undergoes a simple normal shock in the diffuser, its static pressure will be 0.23 atmosphere, and to be conservative it was assumed that the total head of all the flow was reduced to this value.

7. Power Required

An isentropic compression of the fluid will be considered through the compressors so we get, for the power required,

$$P = \dot{m}\, C_p\, T_i \left[\lambda^{\frac{\gamma-1}{\gamma}} - 1 \right]$$

where P = power in kw

$\dot{m}$ = mass flow rate in kg/s

C_p = specific heat at constant pressure = 1 kJ/kg

T_i = intake temperature in ^oK

λ = compression ratio

We will adopt an efficiency of 0.7 for the plant to compute the actual power required.

The arrangements B and C will require compression ratio of 5.30 and 6.15. The results of each stage are shown in the Tables 1 and 2.

Note. To compute the current in the lines we used the relation

$$P = UI\sqrt{3}\cos\phi$$

where

P = power required by the engine (watts)

U = voltage (2300 V)

I = current (A)

$\cos\phi = 0.8$, where ϕ is the phase angle.

The maximum currents are for the following arrangements:

$$2 \times C300 + 2 \times C300H = 2 \times 39 \text{ A}$$

$$C200 + C200H = 19 \text{ A}$$

For each case we can check, the required currents are very much lower than these maximum values.

8. Conclusion

The arrangement C given by Fig. 2 will be adopted because of its better distribution of power. In this case, a very high recovery factor will not be required in the diffuser.

II. DESIGN OF THE NOZZLE

1. Introduction

A double nozzle divided by a plate in its middle is required to separate the two flows before their mixing (Figs. 1 and 8). The upper flow (the supersonic one) must be designed for a mass flow rate of 0.50 kg/s and the lower one for a mass flow rate of 0.27 kg/s. The nozzle is also divided longitudinally into a double convergent nozzle (i.e., one which converges in two directions and is identical for both streams) with an exit Mach number of 0.5 and two-dimensional nozzles which accelerate the two streams respectively to Mach numbers 1.4 and 0.7.

2. The Restriction Section

Wall contours were obtained by fitting a fifth-degree polynomial to six boundary conditions. At the inlet, the slope and curvature were chosen to be zero; the inlet area was chosen to give a small inlet speed ($\sim$10 m/s). The exit conditions were chosen to give a Mach number of 0.5. The slope and curvatures of the walls were chosen to match the corresponding values for the one-dimensional transonic nozzles. The nozzle length was arbitrarily chosen to be 1/2 to minimize secondary flows. See Figs. 8 and 10 for details of the design.

3. Design of the Transonic Nozzle

To simplify the construction of the nozzle, we considered a two-dimensional inlet for the transonic flow to Mach number 1.4 and also a two-dimensional nozzle to accelerate the subsonic stream to Mach number 0.7.

The equation of the wall contour of the transonic part of the nozzle between Mach numbers 0.5 and 1.4 has been determined by Friedrichs' method (see reference 3). The mathematical part of this method was developed by Wilson (see reference 4). The wall contour of the subsonic part of the nozzle will be fitted with a third-degree polynomial after the boundary layer determination. The nozzle design method to be used for the design of the transonic nozzle must have the following properties:

1) it should be capable of absorbing the inlet conditions and the design Mach number and then yielding a uniform flow testing region with the desired accuracy;
2) it should produce a wall contour with continuous second derivatives;
3) the method used must be adaptable to machine computation in order to get a good accuracy for the contour.

The majority of the nozzles are designed using the method of characteristics. However, this method can be used only for supersonic nozzles in the supersonic region. This implies an arbitrary assumption about the flow in the throat and an arbitrary subsonic contour.

The method proposed by Friedrichs does not present any disruption at the sonic conditions and the computation will be available from Mach numbers 0.5 to 1.4.

The object of the method is to construct nozzles through which the flow conditions are known completely; the development begins with

prescribing more or less arbitrarily a velocity distribution along the axis of symmetry of the nozzle. In our case we chose the centerline Mach number distribution as the main parameter.

A flow having this Mach number distribution will be established and the contour will be obtained by considering a particular streamline of this flow. The Friedrichs' method consists of expanding the Cartesian coordinates (x, y), the flow direction (θ) and the velocity ratio ($u/\bar{u}$) in power series of ξ and η which are the equipotentials and streamlines as shown in Fig. 9, and $\bar{u}$ is the velocity on the centerline.

The hydrodynamical equations. The flow is assumed to be steady, irrotational, and isentropic; the viscous effects will be considered later by a boundary layer correction.

The equation of continuity may be written

$$\frac{\partial}{\partial x}(\rho u) + \frac{\partial}{\partial y}(\rho v) = 0 \tag{1}$$

and the condition for irrotationality is

$$\frac{\partial u}{\partial y} - \frac{\partial v}{\partial x} = 0 \ . \tag{2}$$

We can define a potential function ϕ and a stream function ψ, such as

$$\begin{aligned} \phi_x &= u & \qquad \psi_x &= -\rho v \\ \phi_y &= v & \qquad \psi_y &= +\rho u \end{aligned} \tag{3}$$

Note: the method used looks very much like the theory of incompressible flows, but here the compressibility effect appears in ψ, which is a function both of the velocity field (u and v) and ρ. Thus,

$$\begin{aligned} d\phi &= \phi_x dx + \phi_y dy = u \cos\theta \, dx + u \sin\theta \, dy \ , \\ d\psi &= \psi_x dx + \psi_y dy = -\rho u \sin\theta \, dx + \rho u \cos\theta \, dy \ . \end{aligned} \tag{4}$$

Combining these two equations we get

$$dx = \frac{\cos\theta}{u}\, d\phi - \frac{\sin\theta}{\rho u}\, d\psi = \frac{\partial x}{\partial y}\, d\phi + \frac{\partial x}{\partial y}\, d\psi$$

$$dy = \frac{\sin\theta}{u}\, d\phi + \frac{\cos\theta}{\rho u}\, d\psi = \frac{\partial y}{\partial \phi}\, d\phi + \frac{\partial y}{\partial \psi}\, d\psi$$

and

$$\frac{\partial x}{\partial \phi} = \frac{\cos\theta}{u} \quad ; \quad \frac{\partial x}{\partial y} = -\frac{\sin\theta}{\rho u}$$

$$\frac{\partial y}{\partial \phi} = \frac{\sin\theta}{u} \quad ; \quad \frac{\partial y}{\partial \psi} = \frac{\cos\theta}{\rho u}$$

Let us introduce the new variables ξ and η as functions of the velocity distribution $\bar{u}$ along the centerline. Having the equipotential lines ξ = constant and the streamlines η = constant, we get

$$\phi = \int_0^{\xi} \bar{u}(x)\, dx \qquad \text{and} \qquad \psi = \rho^* u^* \eta \tag{5}$$

where (*) describes the critical conditions (M = 1.0).

The partial derivatives of x and y with respect to those new variables are

$$\frac{\partial x}{\partial \xi} = \frac{\partial x}{\partial \phi} \cdot \frac{d\phi}{d\xi} = \frac{\cos\theta}{u} \cdot \bar{u} \quad ; \quad \frac{\partial x}{\partial \eta} = \frac{\partial x}{\partial \psi} \cdot \frac{d\psi}{d\eta} = \frac{-\sin\theta}{\rho u} \cdot \rho^* u^*$$

and

$$\frac{\partial y}{\partial \xi} = \frac{\partial y}{\partial \phi} \cdot \frac{d\phi}{d\xi} = \frac{\sin\theta}{u} \cdot \bar{u} \quad ; \quad \frac{\partial y}{\partial \eta} = \frac{\partial y}{\partial \psi} \cdot \frac{d\psi}{d\eta} = \frac{\cos\theta}{\rho u} \cdot \rho^* u^* \tag{6}$$

Forming the cross-partial derivatives and eliminating x and y from these equations we get

$$\frac{\partial}{\partial \eta}\left(\frac{\bar{u}}{u}\cos\theta\right) = \frac{\partial^2 x}{\partial \eta \partial \xi} = \frac{\partial^2 x}{\partial \xi \partial \eta} = -\frac{\partial}{\partial \xi}\left(\frac{\rho^* u^*}{\rho u}\sin\theta\right)$$

and (7)

$$\frac{\partial}{\partial \eta}\left(\frac{\bar{u}}{u}\sin\theta\right) = \frac{\partial^2 y}{\partial \eta \partial \xi} = \frac{\partial^2 y}{\partial \xi \partial \eta} = \frac{\partial}{\partial \xi}\left(\frac{\rho^* u^*}{\rho u}\cos\theta\right)$$

but $\rho^* u^* / \rho u = A/A^*$: the area ratio enters by means of the continuity of mass which also may be written h because of the one-dimensional

analysis. Hence, by expanding (7),

$$\cos\theta \frac{\partial}{\partial\eta}\left(\frac{\bar{u}}{u}\right) - \frac{\bar{u}}{u}\sin\theta\frac{\partial\theta}{\partial\eta} = -h\cos\theta\frac{\partial\theta}{\partial\xi} - \sin\theta\frac{\partial h}{\partial\xi}$$

$$\sin\theta \frac{\partial}{\partial\eta}\left(\frac{\bar{u}}{u}\right) + \frac{\bar{u}}{u}\cos\theta\frac{\partial\theta}{\partial\eta} = -h\sin\theta\frac{\partial\theta}{\partial\xi} + \cos\theta\frac{\partial h}{\partial\xi} \qquad (8)$$

Combining these two equations we get

$$\frac{\partial}{\partial\eta}\left(\frac{\bar{u}}{u}\right) = -h\frac{\partial\theta}{\partial\xi} \qquad (9)$$

and

$$\frac{\bar{u}}{u}\frac{\partial\theta}{\partial\eta} = \frac{\partial h}{\partial\xi} \; . \qquad (10)$$

These partial differential equations may be solved by expressing x, y, u, θ as power series of η with coefficients which are functions of ξ.

Derivation of the series representations. The flow is restricted to be symmetric with respect to the x-axis. Then the center line can be taken as the streamline $\eta = 0$.

The variable x, therefore, is an even function of η equal to ξ at the centerline. Hence

$$x = \xi + x_2(\xi)\eta^2 + x_4(\xi)\eta^4 + \ldots \; . \qquad (11)$$

The flow field is also an even function of η, so

$$\frac{u}{\bar{u}} = 1 + \delta_2(\xi)\eta^2 + \ldots \qquad (12)$$

but ϕ and θ will be, because of the coordinate choice, odd functions of η, so

$$y = y_1(\xi)\eta + y_3(\xi)\eta^3 + \ldots \qquad (13)$$

and

$$\theta = \theta_1(\xi)\eta + \theta_3(\xi)\eta^3 + \ldots \; . \qquad (14)$$

The coefficients of these series expansions are determined by the

particular choice of the velocity distribution $\bar{u}(x)$ on the centerline.

But it is more convenient to express these coefficients in terms of the area ratio (h) or the Mach number distribution $\bar{M}$ at the centerline.

From Appendix A,

$$\frac{h}{\bar{h}} = \frac{\bar{u}}{u}\left(\frac{\frac{\gamma+1}{2} - \frac{\gamma-1}{2}\left(\frac{\bar{u}}{u^*}\right)^2}{\frac{\gamma+1}{2} - \frac{\gamma-1}{2}\left(\frac{u}{u^*}\right)^2}\right)^{\frac{1}{\gamma-1}}$$

and assuming the power series expansion (12),

$$\frac{u}{\bar{u}} = 1 + \delta_2(\xi)\eta^2 + \dots \quad ,$$

we get

$$\frac{h}{\bar{h}} = (1+\delta_2(\xi)\eta^2+\dots)^{-1}\left(\frac{\frac{\gamma+1}{2} - \frac{\gamma-1}{2}\left(\frac{u}{u^*}\right)^2(1+\delta_2\eta^2+\dots)^2}{\frac{\gamma+1}{2} - \frac{\gamma-1}{2}\left(\frac{\bar{u}}{u^*}\right)^2}\right)^{-\frac{1}{\gamma-1}}$$

so

$$\frac{h}{\bar{h}} = (1-\delta_2\eta^2+\dots)\left(1 - \frac{(\gamma-1)\bar{u}^2}{(\gamma+1)u^{*2}-(\gamma-1)\bar{u}^2}\cdot 2\delta_2\eta^2+\dots\right)^{-\frac{1}{\gamma-1}} \quad .$$

$$= 1 + \left(\frac{2\bar{u}^2}{(\gamma+1)u^{*2}-(\gamma-1)\bar{u}^2} - 1\right)\delta_2\eta^2+\dots \quad .$$

But from Appendix A,

$$\bar{M}^2 = \frac{2\bar{u}^2}{(\gamma+1)u^{*2}-(\gamma-1)\bar{u}^2} \quad ,$$

so

$$\frac{h}{\bar{h}} = 1 + \delta_2\cdot(\bar{M}^2-1)\eta^2 + \dots \quad . \qquad (15)$$

From the last equation of (6)

$$\frac{\partial y}{\partial \eta} = \cos\theta\, h \ .$$

Assuming θ small we get

$$\cos\theta = 1 - \frac{\theta^2}{2} + \ldots \quad ,$$

but from (14),

$$\theta = \theta_1(\xi)\eta + \theta_3(\xi)\eta^3 + \ldots \ .$$

Keeping the second order terms we get

$$\frac{\partial y}{\partial \eta} = \bar{h}\cdot\left(1+\delta_2(\bar{M}^2-1)\eta^2+\ldots\right)\cdot\left(1-\frac{\theta_1^2}{2}\eta^2+\ldots\right)$$

$$= \bar{h}\left(1+\eta^2\left[\delta_2(\bar{M}^2-1)-\frac{\theta_1^2}{2}\right]+\ldots\right) \quad , \tag{16}$$

but from (13),

$$y = y_1(\xi)\eta + y_3(\xi)\eta^3 + \ldots \ .$$

After differentiation with respect to η

$$\frac{\partial y}{\partial \eta} = y_1(\xi) + 3y_3(\xi)\eta^2 + \ldots \ . \tag{17}$$

After identification with (16) we obtain

$$y_1 = \bar{h} \tag{18}$$

$$y_3 = \frac{\bar{h}}{3}\left(\delta_2(\bar{M}^2-1)-\frac{\theta_1^2}{2}\right) \ . \tag{19}$$

From equation (9)

$$\frac{\partial}{\partial\eta}\left(1+\delta_2\eta^2+\ldots\right)^{-1} = -\bar{h}\left(1+\delta_2(\bar{M}^2-1)\eta^2+\ldots\right)\frac{\partial}{\partial\xi}\left(\theta_1\eta+\theta_3\eta^3+\ldots\right) \ ,$$

or, after differentiation,

$$-2\delta_2\eta + \ldots = -\bar{h}\left(1+\delta_2(\bar{M}^2-1)\eta^2+\ldots\right)\left(\theta_1'\eta+\theta_3'\eta^3+\ldots\right) \ ,$$

where primes denote differentiation with respect to ξ .

Equating first order terms we get

$$\delta_2 = \tfrac{1}{2}\bar{h}\theta_1' \quad . \tag{20}$$

From equation (10) we have

$$\frac{\partial\theta}{\partial\eta} = \left(\frac{u}{\bar{u}}\right)\frac{\partial h}{\partial\xi} \quad ,$$

so

$$\theta_1+3\theta_3\eta^2 = (1+\delta_2\eta^2+\dots)\cdot\frac{\partial}{\partial\xi}\left[\bar{h}(1+\delta_2(\bar{M}^2-1)\eta^2+\dots\right]$$

$$= h'+\eta^2\left[h'\delta^2+\frac{d}{d\xi}\left[\bar{h}\delta_2(\bar{M}^2-1)\right]\right] \quad .$$

Therefore,

$$\theta_1 = \bar{h}' \quad , \tag{21}$$

and

$$\theta_3 = \frac{1}{3}\left(\bar{h}'\delta_2+\frac{d}{d\xi}\bar{h}\,\delta_2(\bar{M}^2-1)\right] \tag{22}$$

so from (20) and (21)

$$\delta_2 = \tfrac{1}{2}\,\bar{h}\,\bar{h}'' \quad ,$$

and from (19)

$$y_3 = \frac{\bar{h}}{6}\left[(\bar{M}^2-1)\bar{h}\,\bar{h}''-\bar{h}'^2\right] \quad .$$

By Appendix A

$$\bar{h} = \frac{u^*}{\bar{u}}\left(\frac{\gamma+1}{2}-\frac{\gamma-1}{2}\left(\frac{\bar{u}}{u^*}\right)^2\right)^{-\frac{1}{\gamma-1}}$$

and

$$\bar{M}^2 = \frac{2\bar{u}^2}{(\gamma+1)u^{*2}-(\gamma-1)\bar{u}^2} = \frac{2}{(\gamma+1)\left(\frac{u^*}{\bar{u}}\right)^2-(\gamma-1)} \quad ,$$

so

$$\left(\frac{u^*}{\bar{u}}\right)^2 = \frac{2+(\gamma-1)\bar{M}^2}{(\gamma+1)\bar{M}^2}$$

and

$$\bar{h} = \frac{1}{\bar{M}}\left[\frac{(\gamma-1)\bar{M}^2+2}{\gamma+1}\right]^{\frac{\gamma+1}{2(\gamma-1)}} .$$

After differentiation

$$2\bar{M}\bar{M}^2 = \frac{(\gamma-1)\bar{M}^2+2}{(\bar{M}^2-1)}\ \bar{M}^2\frac{\bar{h}'}{\bar{h}} .$$

Thus, from (22),

$$\theta_3 = \frac{1}{6}\bar{h}\bar{h}'\bar{h}'' + \frac{1}{6}\frac{d}{d\xi}\left[\bar{h}^2\bar{h}''(\bar{M}^2-1)\right] ,$$

so

$$\theta_3 = \frac{1}{6}\bar{h}\bar{h}'\bar{h}''\left[\frac{(\gamma+1)\bar{M}^4}{\bar{M}^2-1} - 1\right] + \frac{1}{6}\bar{h}^2\bar{h}'''(\bar{M}^2-1) .$$

Using the second equation of (6) and the approximation $\sin\theta = \theta - \frac{\theta^3}{6} + \ldots$, we get

$$\frac{\partial x}{\partial \eta} = -\bar{h}\left[\theta - \frac{\theta^3}{6} + \ldots\right] ,$$

so

$$2x_2\eta + 4x_4\eta^3 = -\bar{h}\eta\left\{\theta_1+\left[\delta_2\theta_1(\bar{M}^2-1)+\theta_3-\frac{\theta_1^3}{6}\right]\eta^2+\ldots\right\} .$$

After identification

$$x_2 = -\tfrac{1}{2}\bar{h}\bar{h}' ,$$

and

$$x_4 = -\frac{\bar{h}}{4}\left[\delta_2\theta_1(\bar{M}^2-1)+\theta_3-\frac{\theta_1^3}{6}\right] .$$

Now assuming higher order expansions

$$y = y_1(\xi)\eta + y_3(\xi)\eta^3 + y_5(\xi)\eta^5 + \ldots$$

$$\theta = \theta_1(\xi)\eta + \theta_3(\xi)\eta^3 + \theta_5(\xi)\eta^5 + \ldots$$

$$\frac{u}{\bar{u}} = 1 + \delta_2(\xi)\eta^2 + \delta_4(\xi)\eta^4 + \ldots .$$

Considering the differential equations (9), (10), and (8), after differ-

entiation with respect to ξ and identification we get

$$\delta_4 = \frac{1}{8}\bar{h}^2\bar{h}''^2(\bar{M}^2+1) + \frac{1}{4}\bar{h}\theta_3'$$

$$y_5 = \frac{1}{5}\bar{h}\left[\frac{1}{8}\bar{h}^2\bar{h}''^2(\gamma\bar{M}^4-\bar{M}^2+2) + \delta_4(\bar{M}^2-1) - \frac{1}{4}\bar{h}\bar{h}'^2\bar{h}''(\bar{M}^2-1) - \bar{h}'\theta_3 + \frac{\bar{h}'^4}{24}\right]$$

$$\theta_5 = \frac{\bar{M}}{5}\delta_4(\bar{h}'\bar{M}+2\bar{h}\bar{M}') + \frac{\bar{h}\bar{h}''}{20}(6\theta_3 - \bar{h}\bar{h}'\bar{h}'') + \frac{1}{40}\bar{h}^2\bar{h}''(3\bar{h}'\bar{h}''+2\bar{h}\bar{h}''')(\gamma\bar{M}^4-\bar{M}^2+2)$$

$$+ \frac{1}{20}\bar{h}^3\bar{h}''^2\bar{M}\bar{M}'(2\gamma\bar{M}^2-1) + \frac{1}{5}\bar{h}\delta_4'(\bar{M}^2-1)$$

and where

$$\theta_3' = \frac{1}{6}(\bar{h}'^2\bar{h}''+\bar{h}\bar{h}''^2+\bar{h}\bar{h}'\bar{h}''')\left\{\frac{(\gamma+1)\bar{M}^4}{\bar{M}^2-1} - 1\right\} + \frac{1}{3}(\gamma+1)\bar{h}\bar{h}'\bar{h}''\bar{M}'\bar{M}^3\frac{\bar{M}^2-2}{(\bar{M}^2-1)^2}$$

$$+ \frac{1}{6}\bar{h}(2\bar{h}'\bar{h}'''+\bar{h}\bar{h}'''')(\bar{M}^2-1) + \frac{1}{3}\bar{h}^2\bar{h}'''\bar{M}'\bar{M} \quad .$$

Determination of the wall contour. One specific value of η has to be chosen to determine the contour wall.

At the throat for the critical conditions we have

$$\psi = \rho^* u^* \eta \quad ,$$

and at the exit of the nozzle

$$\psi = \bar{\rho}_t \bar{u}_t y_t \quad ,$$

so

$$\rho^* u^* \eta = \bar{\rho}_t \bar{u}_t y_t \qquad (t \text{ for test section}) \; .$$

Hence,

$$\eta = \frac{\bar{\rho}_t \bar{u}_t}{\rho^* u^*} y_t = \frac{1}{\bar{h}_t} \cdot y_t \quad .$$

By definition,

$$h = \frac{A}{A^*} = \frac{\rho^* u^*}{\rho u} = \frac{1}{M}\left[\frac{(\gamma-1)M^2+2}{\gamma+1}\right]^{\frac{\gamma+1}{2(\gamma-1)}}$$

$$\therefore \quad \eta = y_t/\bar{h}_t \quad .$$

In our case, y_t will be equal to 50 mm and $\bar{h}_t$, the area ratio corresponding to Mach number 1.4, is 1.115.

Choice of the centerline Mach number distribution. The function used for the centerline distribution has to be analytic in order that the high order derivatives will exist. Obviously, the Mach number must equal one at the throat and 1.4 downstream of the splitter plate. In reference [17] it is shown that continuous derivatives of order (n) for the centerline Mach number distribution produce a wall contour with continuous derivatives of order (n+1). In our case, continuous derivatives are required to the third order for the contour, which means we will need at least $\bar{M}'_t = \bar{M}''_t = 0$ for the test section entrance.

It seems reasonable that the Mach number along the nozzle contour wall should also be a smooth, monotonically increasing function. A source flow provides such a function for part of the supersonic contour, but it does not satisfy the boundary conditions $\bar{M}'_t = \bar{M}''_t = 0$.

However, we will take such a distribution up to the intermediate Mach number 1.2. Between this value and the test section value, we will fit the distribution by a 9th order polynomials satisfying the boundary conditions to the fifth order derivatives at both Mach number 1.2 and 1.4 (see Fig. 10).

Between 0.5 and 1.2, the equation for the centerline Mach number distribution is:

$$\xi = \frac{\bar{M}^m - 1}{\bar{M}} \left[\frac{x_t \bar{M}_t}{\bar{M}_t^m - 1} - k(\bar{M}_t - \bar{M})^{\frac{1}{n}} \right]$$

where m and n are integers and k a real positive number, with the

restrictions that

$$m > 0$$

$$n \geq 3$$

$$k < \frac{x_t M_t^{\frac{1}{1-n}}}{\bar{M}_t^m - 1} \quad ,$$

to assure continuity and at least continuity for the second derivatives.

In our case, we chose:

$$m = 2$$

$$n = 3$$

$$k = 1 \text{ inch} = 25.4 \text{ mm}$$

$$x_t = 10 \text{ inches} = 254 \text{ mm} .$$

The centerline distribution between 1.2 and 1.4 will be automatically fitted with a 9th order polynomial in the computer program.

The results for the double convergent nozzle (to Mach number 0.5) and the transonic nozzle are shown in Tables 5 and 6. The method used to compute the subsonic nozzle between Mach numbers 0.5 and 0.7 will be described further after the boundary layer analysis.

Computer program to design the nozzle (Tables 3 and 4).

Friedrich's method was used between Mach number 0.5 and 1.4. To Mach number 0.5 a double convergent nozzle was computed using 5th order polynomials to represent the wall contours. Thus, we have the following schedule.

x_{mm}	Mach Number	Method Used	Centerline Mach Number Distribution
$0 \le x \le 350$	$0 \le \bar{M} \le 0.5$	polynomial wall contour double convergent	determined from the contours
$350 \le x \le 600$	$0.5 \le \bar{M} \le 1.2$	Friedrichs' method	$\xi = \frac{\bar{M}^n - 1}{\bar{M}} \left[\frac{x_t \bar{M}_t}{\bar{M}_t - 1} - k(\bar{M}_t - \bar{M}) \right]^{\frac{1}{n}}$
$600 \le x \le 720$	$1.2 \le \bar{M} \le 1.4$	Friedrichs' method	9th order polynomial
$x \ge 720$	$\bar{M} = 1.4 =$ constant	constant properties of the flow	$\bar{M} = 1.4 =$ constant

The derivatives to the fourth order of the area ratio ($\bar{h}$) as functions of the derivatives of the centerline Mach number distribution are given in Appendix B. In Appendix C we will find the derivatives of the inverse function $\bar{M}(\xi)$ as a function of $\xi(\bar{M})$ and the derivatives of the Mach number distribution.

4. Conclusion

The Friedrichs' method gives us a very smooth wall contour and a constant Mach number distribution downstream of the splitter plate. This theoretical wall contour will now be modified to take account of the boundary layer.

The input of the first part of the computer program (Friedrichs' method), y, dy/dx, $\bar{M}$, $d\bar{M}/dx$, will be used directly for the computation of the boundary layer correction. The displacement thickness

(δ^*) will be calculated and the nozzle contour used in constructing the nozzle will be obtained by adding values of δ^* to the contour calculated by the Friedrichs' method. The subsonic nozzle (between 0.5 and 0.7) will be computed from this new wall contour after boundary layer correction.

III. BOUNDARY LAYER CORRECTION

1. Introduction

In the previous chapter the boundary layer effect was not taken into account in the calculation of the nozzle wall contour. The boundary layer displacement thickness (δ^*) characterizing the deficit of mass flow rate due to the boundary layer is the parameter usually used to compute the actual wall contour. To keep the computed Mach number distribution, the actual flow section will be obtained by adding the product of $\delta^* \cdot p$ (where p is the perimeter of the flow section) to the value of flow section previously calculated.

Because of the constant thickness of the splitter plate and the constant width of the test section, all the correction will be applied to the top and bottom walls of the nozzle block.

The interaction of the shock waves with the boundary layer was not considered in this simple computation of the displacement thickness. The main flow will be assumed isentropic, compressible, and with a pressure gradient; it will be characterized by the centerline Mach number distribution previously chosen.

The velocity profile of the turbulent boundary layer will be described by the following defect law (see reference 15):

$$\frac{\overline{U}-u}{u_\tau} = -\frac{1}{K}\,\mathrm{Log}\left(\frac{y}{\delta}\right) + \frac{\tilde{\pi}(x)}{K}\left[2-w\left(\frac{y}{\delta}\right)\right]$$

with $\overline{U}$: mean velocity at the centerline

u : velocity in the boundary layer

u_τ : defined as $\sqrt{\frac{\tau_w}{\rho}}$, friction velocity

K : Karman's constant = 0.41

δ : boundary layer thickness

$\tilde{\pi}$: Coles' parameter for the wake component of the boundary layer

$w(\frac{y}{\delta})$: Coles' wake component function, usually $w(\frac{y}{\delta}) = 1 + \cos(\pi \frac{y}{\delta})$

The integration of the differential equation giving θ will be performed numerically on the computer by using 4th order Runge-Kutta's method.

2. Compressible Boundary Layer Function of the Wall Contour and the Mach Number Distribution

The coordinates the the notations used in this chapter are shown on Fig. 14. Let us now write the basic equations for the boundary layer:

- equation of continuity

$$\frac{\partial}{\partial x}(B\rho u) + \frac{\partial}{\partial y}(B\rho v) = 0 \qquad (1)$$

- momentum in the x direction

$$\rho u \frac{\partial u}{\partial x} + \rho v \frac{\partial u}{\partial y} = - \frac{dP}{dx} + \frac{\partial \tau}{\partial y} \quad . \qquad (2)$$

Immediately outside the boundary layer $u = \overline{U}$ and also $\partial \overline{U}/\partial y = 0$, to the scale of the boundary layer thickness. Therefore,

$$\rho_e \overline{U} \frac{d\overline{U}}{dx} = - \frac{dP}{dx} \quad ,$$

so that (2) becomes

$$\rho u \frac{\partial u}{\partial x} + \rho v \frac{\partial u}{\partial y} = \rho_e \bar{U} \frac{d\bar{U}}{dx} + \frac{\partial \tau}{\partial y} \tag{3}$$

The core flow is adiabatic so that

$$Tt = To = \text{constant} \tag{4}$$

If we introduce the velocity defect in the x-direction $(\bar{U}-u)$ and the x-momentum defect, $(\rho_e \bar{U} - \rho u)$, we obtain from (3)

$$(\rho_e \bar{U} - \rho u)\frac{\partial \bar{U}}{\partial x} + \rho u \frac{\partial}{\partial x}[\bar{U}-u] - \rho v \frac{\partial}{\partial y}(\bar{U}-u) = -\frac{\partial \tau}{\partial y} \quad . \tag{5}$$

Multiply (1) by $(\bar{U}-u)$ and (5) by B(x) and add to get:

$$B(x)[\rho_e \bar{U}-\rho u]\frac{\partial \bar{U}}{\partial x} + \frac{\partial}{\partial x}\left[B(x)\rho u[\bar{U}-u]\right] - \frac{\partial}{\partial y}[B(x)\rho v(\bar{U}-u)] = -B(x)\frac{\partial \tau}{\partial y} \tag{6}$$

where B(x) is the cross-section distribution.

Integrate (6) with respect to y from 0 to δ and use the conditions that $u(x, 0) = 0$ and $u(x, \delta) = \bar{U}(x)$. The result is:

$$B(x)\frac{\partial \bar{U}}{\partial x}\int_0^\delta [\rho_e \bar{U}-\rho u]dy + \frac{\partial}{\partial x} B(x) \int_0^\delta \rho u(\bar{U}-u)dy = B(x)\tau_w \tag{7}$$

Note

$$-\int_0^\delta \frac{\partial \tau}{\partial y}\, dy = -(\tau_\delta - \tau_o) = \tau_w \quad .$$

When we introduce the integral parameters

$$\delta^* = \int_0^\delta \left(1 - \frac{\rho u}{\rho_e \bar{U}}\right)dy \quad \text{and} \quad \theta = \int_0^\delta \frac{\rho u}{\rho_e \bar{U}}\left(1 - \frac{u}{\bar{U}}\right)dy \ ,$$

we get

$$B(x) \frac{d\bar{U}}{dx} \rho_e \bar{U} \delta^* + \frac{d}{dx}\left[B(x) \rho_e \bar{U}^2 \theta\right] = B(x) \tau_w \qquad (8)$$

and after expanding the second term:

$$B(x) \frac{d\bar{U}}{dx} \rho_e \bar{U}\delta^* + B(x) \rho_e \bar{U}^2 \frac{d\theta}{dx}\left[B(x) \rho_e u^2\right] = B(x) \tau_w \quad . \qquad (9)$$

After dividing by $B(x) \rho \bar{U}^2$ and introducing the shear wall coefficient $C_f = \frac{\tau w}{\frac{\rho_e u^2}{2}}$, we get:

$$\frac{1}{\bar{U}} \frac{d\bar{U}}{dx} \delta^* + \frac{d\theta}{dx} + \frac{\theta}{B \rho_e \bar{U}^2} \frac{d}{dx}\left[B \rho_e \bar{U}^2\right] = \frac{\tau_w}{\rho_e \bar{U}^2} = \frac{1}{2} C_f . \qquad (10)$$

But $\rho_e = \rho_t \left[1 + \frac{\gamma-1}{2} \bar{M}^2\right]^{\frac{-1}{\gamma-1}}$,

so

$$\frac{1}{\rho_e} \frac{d\rho_e}{dx} = -\frac{\bar{M}^2}{\bar{U}} \frac{d\bar{U}}{dx}$$

and $\bar{U} = \bar{M}a = \bar{M}\sqrt{\gamma R T}$

with $T = T_t \left(1 + \frac{\gamma-1}{2} \bar{M}^2\right)^{-1}$,

so $\frac{1}{\bar{U}} \frac{d\bar{U}}{dx} = \frac{1}{1 + \frac{\gamma-1}{2} \bar{M}^2} \frac{1}{\bar{M}} \frac{d\bar{M}}{dx}$.

Hence, after introducing $H = \frac{\delta^*}{\theta}$, (10) becomes

$$\frac{d\theta}{dx} + \theta \left[\frac{2+H-\bar{M}^2}{1+\frac{\gamma-1}{2} \bar{M}^2} \frac{d\bar{M}}{\bar{M}\,dx} + \frac{dB}{B dx}\right] = \frac{1}{2} C_f \quad . \qquad (11)$$

In the case of incompressible flow, with a 1/7 th power velocity distribution law for the boundary layer which leads to H = 1.28, equation (11) might be integrated directly. In our case we must assume a more complex velocity profile which will give us values for H and C_f. For this purpose we introduce the Howarth transformation,

$$y_i = \int_0^y \frac{\rho}{\rho_e}\, d\eta \qquad \text{so} \qquad dy_i = \frac{\rho}{\rho_e}\, dy \ .$$

Then the integral parameters become

$$\delta^* = \int_0^{\delta} \left(1 - \frac{\rho u}{\rho_e \bar{U}}\right) dy = \int_0^{\delta_i} \left(\frac{\rho_e}{\rho} - \frac{u}{\bar{U}}\right) dy_i \ .$$

Across the boundary layer

$$P \simeq \text{constant, so } \frac{\rho_e}{\rho} = \frac{T_e}{T} \ ,$$

and assuming constant total temperature

$$C_p T_e + \tfrac{1}{2} \bar{U}^2 = C_p T + \tfrac{1}{2} u^2$$

we get

$$\frac{T}{T_e} = 1 + \frac{1}{2} \frac{\bar{U}^2}{C_p T_e} \left(1 - \frac{u^2}{\bar{U}^2}\right) = 1 + \frac{\gamma - 1}{2} \bar{M}^2 \left(1 - \frac{u^2}{\bar{U}^2}\right)$$

and

$$\left(\frac{\rho_e}{\rho} - \frac{u}{\bar{U}}\right) = \left(1 + \frac{\gamma - 1}{2} \bar{M}^2\right)\left(1 - \frac{u^2}{\bar{U}^2}\right) + \frac{\gamma - 1}{2} \bar{M}^2 \frac{u}{\bar{U}} \left(1 - \frac{u}{\bar{U}}\right) ,$$

which gives for δ^*

$$\delta^* = \left(1 + \frac{\gamma - 1}{2} \bar{M}^2\right) \int_0^{\delta_i} \left(1 - \frac{u^2}{\bar{U}^2}\right) dy_i + \frac{\gamma - 1}{2} \bar{M}^2 \int_0^{\delta_i} \frac{u}{\bar{U}} \left(1 - \frac{u}{\bar{U}}\right) dy_i$$

or

$$\delta^* = \left(1 + \frac{\gamma - 1}{2} \bar{M}^2\right) \delta_i^* + \frac{\gamma - 1}{2} \bar{M}^2 \theta_i \ . \qquad (12)$$

With the same transformation of coordinates, we get

$$\theta = \theta_i \quad . \tag{13}$$

Equation (11) may be written

$$\frac{d\theta_i}{dx} + \theta_i\left[\left(2 + H_i - \frac{\gamma+1}{2}\frac{\bar{M}^2}{(1+\frac{\gamma-1}{2}\bar{M}^2)}\right)\frac{d\bar{M}}{\bar{M}\,dx} + \frac{dB}{B dx}\right] = \tfrac{1}{2}C_f \tag{14}$$

where

$$H_i = \frac{\delta_i^*}{\theta_i} \quad .$$

Let us now assume the velocity profile in the incompressible boundary layer given by the velocity defect law (ref. 15):

$$\frac{u}{u_\tau} = f\left(\frac{y_i u_\tau}{\nu}\right) + \frac{\pi(x)}{K}\, w\left(\frac{y_i}{\delta_i}\right)$$

where

$$u_\tau^2 = \frac{\tau_w}{\rho} \quad .$$

For the purpose of computing integral properties we can choose

$$f\left(\frac{y_i u_\tau}{\nu}\right) = \frac{1}{K}\left[\log\left(\frac{y_i u_\tau}{\nu}\right) + C\right] ,$$

where K is the Karman's constant = 0.41 ; C = 2.05 ; and

$$\frac{\tilde{\pi}(x)}{K}\, w\left(\frac{y_i}{\delta_i}\right) = \frac{\tilde{\pi}}{K}\left(1 - \cos\frac{\pi y_i}{\delta_i}\right) .$$

Therefore,

$$\frac{u}{u_\tau} = \frac{1}{K}\left[\log\frac{y_i u_\tau}{\nu} + C + \tilde{\pi}\left(1 - \cos\frac{\pi y_i}{\delta_i}\right)\right] . \tag{15}$$

At $y = \delta$ and $u = \bar{U}$, (15) becomes

$$\frac{\bar{U}}{u_\tau} = \frac{1}{K}\left[\log\left(\frac{\delta_i u_\tau}{\nu}\right) + C + 2\tilde{\pi}\right] . \tag{16}$$

Therefore,

$$\frac{\overline{U}-u}{u_{\tau i}} = \frac{1}{K}\left[-\log\frac{y_i}{\delta_i} + \tilde{\pi}\left(1+\cos\frac{\pi y_i}{\delta_i}\right)\right] \quad . \tag{17}$$

We now have

$$\frac{\delta_i^*}{\delta_i} = \int_0^1 \left(1-\frac{1}{\overline{U}}\right)\frac{dy_i}{\delta_i} = \frac{u_\tau}{\overline{U}}\int_0^1\left(\frac{\overline{U}-u}{u_\tau}\right)\frac{dy_i}{\delta_i} \quad .$$

From the velocity profile (17) we obtain

$$\frac{\delta_i^*\overline{U}}{\delta_i u_\tau} = \frac{1+\tilde{\pi}}{K} \quad .$$

So

$$\frac{\delta_i^*}{\delta_i} = f\,\frac{1+\tilde{\pi}}{K}$$

where $f = (u_{\tau i})/\overline{U}$.

Let us now define the value for $H_i = \dfrac{\delta_i^*}{\theta_i}$. We have, in terms of the new variable y_i

$$\frac{\delta_i^*}{\delta_i} = f\,\frac{1+\tilde{\pi}}{K} \quad . \tag{18}$$

We also have

$$\frac{(\delta_i^*-\theta_i)\overline{U}^2}{\delta_i u_{i\tau}^2} = \int_0^1\left(\frac{\overline{U}-u}{u_{i\tau}}\right)^2 d\left(\frac{y_i}{\delta_i}\right) \quad . \tag{19}$$

The particular profile chosen for the velocity will give:

$$\frac{(\delta_i^* - \theta_i)\bar{U}^2}{\delta_i u_{i\tau}^2} = \left[2 + 2\left[1 + \frac{1}{\pi}\,\mathrm{Si}(\pi)\right]\tilde{\pi} + \frac{3}{2}\tilde{\pi}^2\right] \Big/ K^2 \quad , \tag{20}$$

so

$$\frac{\theta_i}{\delta_i} = f\frac{(1+\tilde{\pi})}{K} - \frac{2f^2}{K^2}\left[1 + \left(1 + \frac{\mathrm{Si}(\pi)}{\pi}\right)\tilde{\pi} + \frac{3}{4}\tilde{\pi}^2\right] \tag{21}$$

where

$$\mathrm{Si}(\pi) = \int_0^{\pi} \frac{\sin u}{u}\, du \quad .$$

But we have

$$\int \frac{\sin u}{u}\, du = u - \frac{u^3}{3.3!} + \frac{u^5}{5.5!} = \cdots \quad ,$$

so after computation to the seventh order $\frac{\mathrm{Si}(\pi)}{\pi} = 0.59$, (21) becomes

$$\frac{\theta_i}{\delta_i} = f\,\frac{(1+\tilde{\pi})}{K}\left[1 - \frac{2f[1 + 1.59\tilde{\pi} + 0.75\tilde{\pi}^2]}{K(1+\tilde{\pi})}\right.$$

and

$$H_i = \frac{\delta_i^*}{\theta_i} = \left[1 - \frac{2f[1 + 1.59\tilde{\pi} + 0.75\tilde{\pi}^2]}{K(1+\tilde{\pi})}\right]^{-1} .$$

If we choose $K = 0.40$,

$\tilde{\pi} = 0.56$ (good value for small pressure gradient),

then for $f = 0.03$

we obtain

$$H_i = (1 - 6.81f)^{-1} = 1.25 \quad .$$

The differential equation (14) giving θ_i will become

$$\frac{d\theta_i}{dx} + \theta_i \left[\left(3.25 + \frac{\gamma-1}{2} \frac{\bar{M}^2}{(1+\frac{\gamma-1}{2}\bar{M}^2)} \right) \frac{d\bar{M}}{\bar{M}\,dx} + \frac{dB}{B\,dx} \right] = \frac{1}{2} C_f \qquad (22)$$

We must now find a relation for C_f in the case of an isentropic compressible flow with Mach number effect. We will use the results of Ref. 10 which states that:

$$C_f = 0.246 e^{-1.56 H_i} (Re_\theta)^{-0.268} \left(\frac{T_e}{T_{ref}} \right)^{1.268} \qquad (23)$$

where $$\frac{T_{ref}}{T_e} = \frac{1}{2}\left(\frac{T_w}{T_e} + 1 \right) + 0.22 \left[\frac{T_{aw}}{T_e} - 1 \right] \qquad (24)$$

Given:

$$T_{aw} = T_w = T_o = 300^\circ K$$

we get

$$\frac{T_{ref}}{T_e} = 0.72 \frac{T_o}{T_e} + 0.38$$

but

$$\frac{T_o}{T_e} = 1 + \frac{\gamma-1}{2} \bar{M}^2$$

so

$$\frac{T_{ref}}{T_e} = 1 + 0.144 \bar{M}^2$$

We also have

$$Re_\theta = \frac{\bar{u}\,\theta}{\nu_{ref}} = \frac{\theta \bar{M} \sqrt{\gamma R T_e}}{\nu_{ref}} = \sqrt{\gamma R} \cdot \frac{\bar{M}}{\nu_{ref}} \cdot \left(\frac{T_o}{1+\frac{\gamma-1}{2}\bar{M}^2} \right)^{\frac{1}{2}} \theta$$

but

$$\frac{\nu_{ref}}{\nu_e} = \frac{\mu_{ref}}{\mu_e} \cdot \frac{\rho_e}{\rho_{ref}} \quad \text{with} \quad \frac{\mu_{ref}}{\mu_e} = \left(\frac{T_{ref}}{T_e} \right)^{0.75}$$

If $P_e \simeq P_{ref}$ we get

$$\nu_{ref} = \left(\frac{T_{ref}}{T_e}\right)^{1.75} \nu_e = \left(\frac{T_{ref}}{T_e}\right)^{1.75} \frac{\mu_e}{\rho_e}$$

Introducing $\nu_o = \frac{\mu_o}{\rho_o}$, we obtain

$$\nu_{ref} = \left(\frac{T_{ref}}{T_e}\right)^{1.75} \cdot \left(\frac{T_e}{T_o}\right)^{0.75} \cdot \left(\frac{\rho_o}{\rho_e}\right) \cdot \nu_o$$

and finally

$$\nu_{ref} = \left(\frac{T_{ref}}{T_e}\right)^{1.75} \left(1 + \frac{\gamma-1}{2}\right)^{1.75} \nu_o$$

C_f may now be written

$$C_f = 0.00235\, T_o^{-0.134} \left(1 + \frac{\gamma-1}{2} \bar{M}^2\right)^{0.134} \cdot \bar{M}^{-0.268} \cdot \left(1 + 0.144\, \bar{M}^2\right)^{-1.268} \cdot \nu_{ref}^{0.268}\, \theta^{-0.268}$$

The differential equation (22) may be written in the form

$$\frac{d\theta_i}{dx} + \theta_i f(x) = g(x)\, \theta_i^{-0.268} \qquad (25)$$

This integration may be performed on the computer using Runge-Kutta's method. f(x) and g(x) are defined point by point for every value of x (see Appendix D).

Because of the Howarth's transformation we obtained

$$\delta^* = \left(1 + \frac{\gamma-1}{2} \bar{M}^2\right)\delta_i^* + \frac{\gamma-1}{2} \bar{M}^2\, \theta_i$$

but $\theta_i = \theta$ and $H_i = \frac{\delta_i^*}{\theta_i}$

hence $\delta^* = \left[\left(1 + \frac{\gamma-1}{2} \bar{M}^2\right) H_i + \frac{\gamma-1}{2} \bar{M}^2\right] \theta$

Taking $H_i = 1.25$ we have

$$\delta^* = \left[H_i + \frac{\gamma-1}{2} \bar{M}^2 (H_i+1)\right] \theta$$

so

$$\delta^* = (1.25 + 0.45 \bar{M}^2)\, \theta \quad . \tag{26}$$

The results for θ and δ^* corresponding to the supersonic stream are shown in Tables 7 and 8 and in Figure 15.

The differential equation (25) was integrated numerically up to $x = 1100$ mm; but from $x = 700$ mm a close form solution is available. From $x = 700$ mm (end of the splitter plate) we have $f(x) = 0$ and $g(x) =$ constant $= 0.0011$ so (21) may be written

$$\frac{d\theta}{dx} = 0.0011\, \theta^{-0.268} \quad .$$

We directly obtain after integrating for $x > 700$ mm

$$\theta(x)^{1.268} - \theta(700)^{1.268} = 0.0011 : 1.268(x-700).$$

With $\theta(700) = 0.298$ we get

$$\theta(x) = (1.39510^{-3}\, x - 0.76)^{0.79} \quad . \tag{27}$$

Since (26) where $\bar{M} = 1.4$ from $x = 700$

$$\delta^*(x) = 2.14 \cdot (1.39510^{-3}\, x - 0.76)^{0.79} \quad . \tag{28}$$

We can now use (27) and (28) to determine $\theta(x)$ and $\delta^*(x)$ in the test section up to $x = 1900$ mm. The results for these values of x are enclosed in Table 8 and shown in Figure 15.

3. Computation of the Boundary Layer in the Subsonic Nozzle

To save time, we are going to use an approximative method to

define the boundary layer in the subsonic nozzle. Up to x = 350 mm the two-dimensional restriction nozzles for both streams are similar. The subsonic part of the transonic nozzle, with values of x varying between 350 mm and 455 mm (i.e. a Mach number between .5 and .7), may be transformed into the subsonic one-dimension restriction nozzle, corresponding to the same Mach number distribution, by stretching the x-coordinate (see Figure 16). In this transformation A and B of the supersonic wall contour nozzle respectively become A' and B' of the subsonic nozzle.

Let x' be the new x-coordinate available for the subsonic nozzle. We must have

$$x' = (x-350).\frac{405}{105} + 350 \tag{29}$$

where x is the coordinate corresponding to the supersonic nozzle block.

In this new system the differential equation (25) providing θ_i (or θ) becomes:

$$\frac{d\theta_i}{dx'} + \theta_i f(x') = g(x')\theta_i^{-0.268} \tag{30}$$

but f(x) is proportional to $\frac{d\bar{M}}{dx}$ and $\frac{dB}{dx}$ so we must have $f(x') = \frac{1}{k} f(x)$ where $k = \frac{405}{105}$.

Coming back to the x-coordinate (30) may be written

$$\frac{d\theta_i}{k\,dx} + \theta_i \frac{f(x)}{k} = g(x')\theta^{-0.268} \tag{31}$$

or

$$\frac{d\theta_i}{dx} + f(x).\theta_i = k\, g(x')\,\theta^{-0.268} \tag{32}$$

This equation is exactly the equation (25) where g(x) is replaced by k g(x').

but $$C_f = 0.246e^{-1.56 H_i} (Re_\theta)^{-0.268} \left(\frac{T_e}{T_{ref}}\right)^{1.268} \quad (23)$$

or $$g(x) = 0.00117\, T_o^{-0.134} \left(1 + \frac{\gamma-1}{2} \bar{M}^2\right)^{0.134} . \bar{M}^{-0.268} . \left(1 + 0.144\, \bar{M}^2\right)^{-1.268} . \nu_{ref}^{0.268}$$

where

$$\nu_{ref} = \left(\frac{T_{ref}}{T_e}\right)^{1.75} \left(\frac{T_e}{T_o}\right)^{0.75} \left(\frac{\rho_o}{\rho_e}\right) \nu_o$$

because of the pressure drop in the valve upstream of the subsonic nozzle (Fig. 1) another value must be adopted for ν_o. At the level of the valve ρ_o drops to 0.44 ρ_o to fit the pressure equilibrium downstream in the test section so we get:

ν_{ref} for the subsonic stream equals 2.28 ν_{ref} for the supersonic stream and

$$g'(x) = 2.28\, g(x) .$$

The differential equation (32) becomes

$$\frac{d\theta_i}{dx} + f(x)\theta_i = \frac{405}{105} . 2.28\, g(x)\, \theta^{-0.268} \quad (33)$$

So by multiplying g(x) by 8.42 and by assuming f(x) = 0 for x > 455 we obtained the differential equation for the subsonic nozzle from the equation (25) valid between A and B.

The solution obtained is only a good approximation of the real solution because by stretching the coordinates we assume values for the slope at A' and B' which are slightly diffrent from the real values.

4. Conclusion

This method allowed us to find a good approximation for the boundary layer solution in the subsonic nozzle and in the test section corresponding to the subsonic flow. Using the results shown in Tables 9 and 10 and Figure 17 the real wall contour will be fitted by a 3rd degree polynomial providing the exact geometric boundary conditions to the first order at A' and B'. At B' the slope will be chosen equal to the boundary layer growing rate in the test section found by the previous solution.

We have for the subsonic nozzle-block: (see Figure 16)

at A' $x = 350$ mm

$y = 67.35$ mm

$y' = 12.10^{-2}$

at B' $x = 755$ mm

$y = 54.00$ mm

$y' = -6.10^{-3}$

The coordinates of the contour wall of the subsonic inlet are shown in Table 11 .

IV. THE MIXING ZONE

Downstream of the splitter plate the characteristics of the two jets are: (see Fig. 18)

1) for the supersonic stream

$\bar{M} = 1.4$, $T = 210^{\circ}K$, $a_1 = 290$ m/s, $v_1 = 405$ m/s, $\rho_1 = 0.43\ \rho_{ot}$

2) for the subsonic stream

$\bar{M} = 0.7$, $T = 270^{\circ}K$, $a_2 = 328$ m/s, $v_2 = 229$ m/s, $\rho_2 = 0.35\ \rho_{ot}$

If b is the thickness of the zone of mixing, we can define the non-dimensional parameter $\bar{b} = \frac{b}{x}$ where x is the x-coordinate starting from the edge of the plate (see ref. 16).

Using Abramovich's formulation available for compressible turbulent jet we get

$$\bar{b} = \frac{b}{x} = C\left(\frac{1+\bar{\rho}}{2}\right)\left(\frac{1-m}{1+\bar{\rho}m}\right)$$

where C = constant = 0.27

$m = \bar{U}_2/\bar{U}_1$

$\bar{\rho} = \rho_2/\rho_1$

so in our case

$m = 0.565$

$\bar{\rho} = 0.81$

so $\bar{b} = b/x = 0.074x$

Because the stagnation temperatures and speeds of the two jets are equal we can suppose with good approximation that the mixing zone will be symmetrical with respect to the x axis defined by the splitter plate.

From Abramovich's theory we now can define the geometry of the mixing zone (see Fig. 18) by:

$$z = \frac{y-y_2}{y_1-y_2} = \frac{y-y_2}{b}$$

and

$$\Delta\bar{u} = (u_2-u)/(u_2-u_1),$$

and u = constant outside of the mixing zone,

by adopting $\Delta\bar{u} = f(z) = (1-z^{\frac{3}{2}})^2$ we get a relationship between x, b and the velocity profile in the jet (see Table 13). By assuming the continuity of mass and the continuity of momentum in the x-direction we can get the velocity profile everywhere in the mixing zone.

So we get

$$\int_{-(h_2+\frac{1}{2}b)}^{(h_1+\frac{1}{2}b)} \rho u\,dy = \rho_1 u_1 h_1(x) + \rho_2 u_2 h_2(x) + \bar{b}x \int_0^1 \rho u\,dz = \text{constant} \quad (1)$$

and

$$\int_{-(h_2+\frac{1}{2}b)}^{(h_1+\frac{1}{2}b)} \rho u^2\,dy = \rho_1 u_1^2 h_1(x) + \rho_2 u_2^2 h_2(x) + \bar{b}x \int_0^1 \rho u^2\,dz = \text{constant} \quad (2)$$

Assuming a zero gradient pressure, we obtain

$$\int_{(-h_2+\frac{1}{2}b)}^{(h_1+\frac{1}{2}b)} \rho u^2\,dy = \frac{1}{R}\int_{(-h_2+\frac{1}{2}b)}^{(h_1+\frac{1}{2}b)} \frac{P}{T}\,u^2\,dy = \gamma \int_{(-h_2+\frac{1}{2}b)}^{(h_1+\frac{1}{2}b)} M^2\,dy = \text{constant.} \quad (3)$$

Again using Abramovich's theory we must define a temperature profile to get the Mach number profile, so we get

$$\Delta T = \frac{T_1-T}{T_1-T_2} \quad \text{so} \quad T = T_1 - \Delta T(T_1-T_2)$$

with $\Delta T = 1 - z$

and by assuming $\Delta P = 0$ we directly have

$$\rho = \frac{P}{RT} = \frac{P}{R[T_1 - \Delta T(T_1 - T_2)]}$$

The different profiles involved in the two equations of continuity are shown in Table 14 and Figures 19 and 20 . By integration of the two integrals (1) and (2) h_1 and h_2 may be determined and also the new height of the test section.

Without boundary layer correction and for x = 1m downstream of the splitter plate the new height of the test section was found equal to 98 mm instead of 100 mm at the edge of the splitter plate (see Figures 19 and 20 . The height-variation due to the mixing zone seems negligible compared to the boundary layer correction. Hence a variable height which may vary between 110m and 120 mm will be adopted at the end of the test section (1150 mm downstream of the splitter plate). A linear variation of the height will also be assumed in the test section starting downstream of the nozzle block (see Fig. 21).

CONCLUSION

The wind tunnel was built from the previous calculations, and all the drawings are retained in the Graduate Aeronautical Laboratories at the California Institute of Technology. However, the main characteristics of the tunnel are shown in the sketches of Fig. 22.

a) Structure

The main structure consists of four beams ($3\frac{1}{2}'' \times 1\frac{1}{2}''$ in cross section) which support the different parts of the nozzle and the test section. These four beams are welded between two flanges and the load is transmitted from the walls of the test section to the beams by eight T-supports located along the test section.

To correct the boundary layer effect and keep a constant pressure in the test section, the height of the test section may be adjusted over $\frac{1}{2}''$ range. This variation is obtained by use of adjustable rails on which the T-supports are supported. These rails are attached to the main beams with bolts and pins.

b) Nozzle Blocks

The supersonic and subsonic nozzle blocks are machined using the X-Y coordinates of the contour given in Tables 11 and 12.

c) Test Section

The top and bottom walls of the test section are segmented in three parts to facilitate the experimental work in the tunnel. The vertical walls are made of glass to allow the visualization of the flow field by using the Schlieren system. A system of movable wedges is used downstream of the test section to adjust the length of the metal walls which support the ends of these two windows.

d) Characteristics of the Wind Tunnel

structure

4 beams, $3\frac{1}{2}'' \times 1\frac{1}{2}'' \times 57\frac{1}{2}''$

4 rails, $1'' \times 1'' \times 49\frac{1}{2}''$

8 T-supports

4 angles

nozzles and test section

supersonic stream, M = 1.4

subsonic stream, M = 0.7

height at the entrance of the test section, 107.20 mm

height at the exit of the test section $\tilde{=}$ 120 mm

length of the test section, 100 cm

width of the test section, 5 cm

experimental devices

pressure probes

Schlieren system

COMPRESSOR ARRANGEMENT B

4 Fuller C300 and 4 Fuller C300H

P_i = 0.21 atmosphere , P_S = 1.1 atmosphere , λ = 5.30

	Compression Ratio	Power Required	Actual Power Required	Current in the Lines
2 x C300	3.08	89 Kw	173 HP	
2 x C300H	1.72	40 Kw	78 HP	
Total	5.30	129 Kw	251 HP	2 x 29 amps

TABLE 1. Results for Compressor Arrangement B

COMPRESSOR ARRANGEMENT C

4 Fuller C300, 4 Fuller C300H, 1 Fuller C200, and 1 Fuller C200H

P_i = 0.18 atmosphere , P_S = 1.1 atmosphere , λ = 6.15

	Compression Ratio	Power Required	Actual Power Required	Current in the Lines
2 x C300	3.10	76 Kw	148 HP	
2 x C300H	1.98	43 Kw	84 HP	2 x 27 amps
C200	2.85	12 Kw	24 HP	
C200H	2.15	6 Kw	12 HP	8 amps
Total	6.15	137 Kw	268 HP	

TABLE 2. Results for Compressor Arrangement C

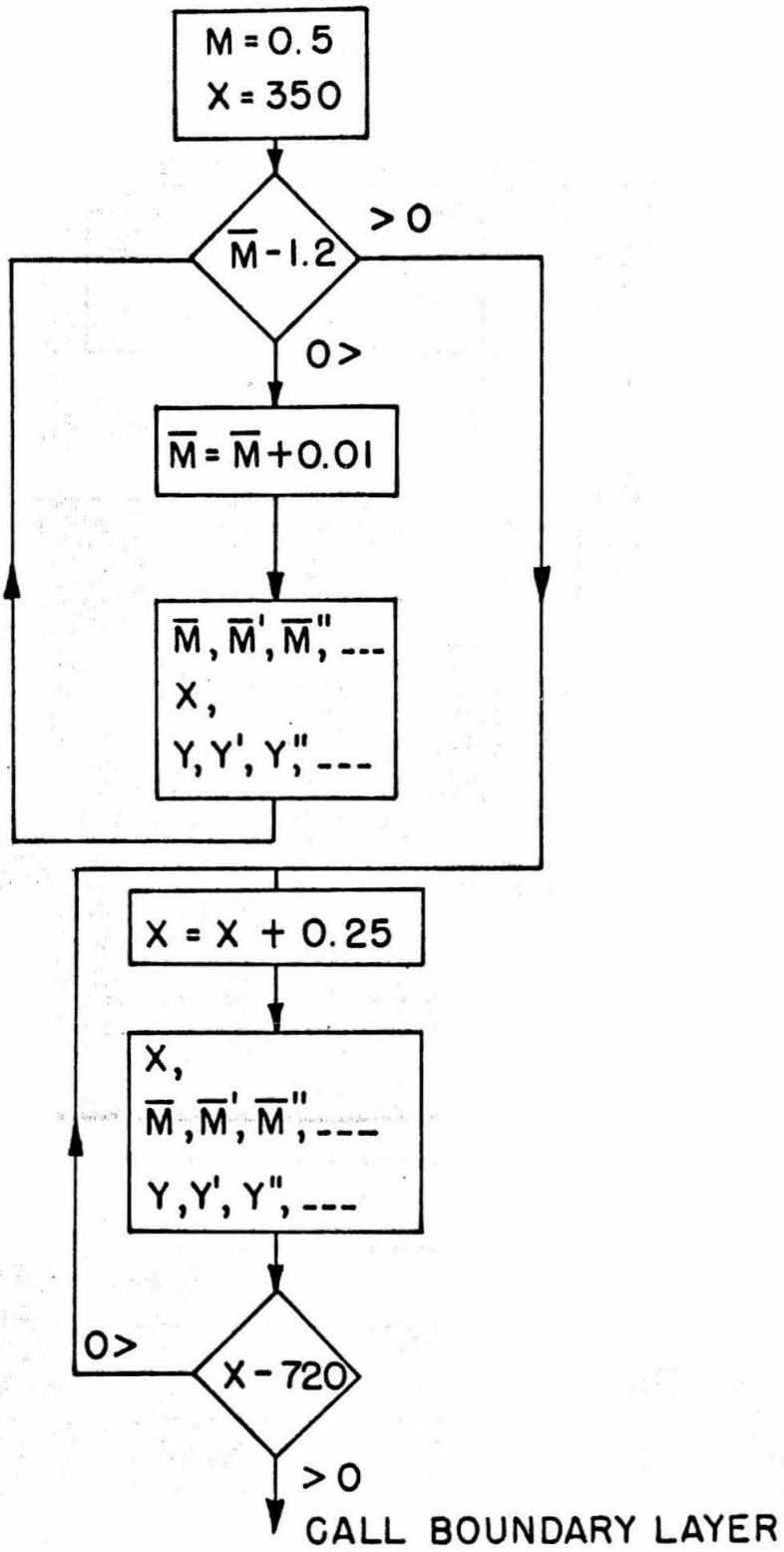

TABLE 3 COMPUTER PROGRAM USED FOR THE FRIEDRICHS' METHOD DESIGN

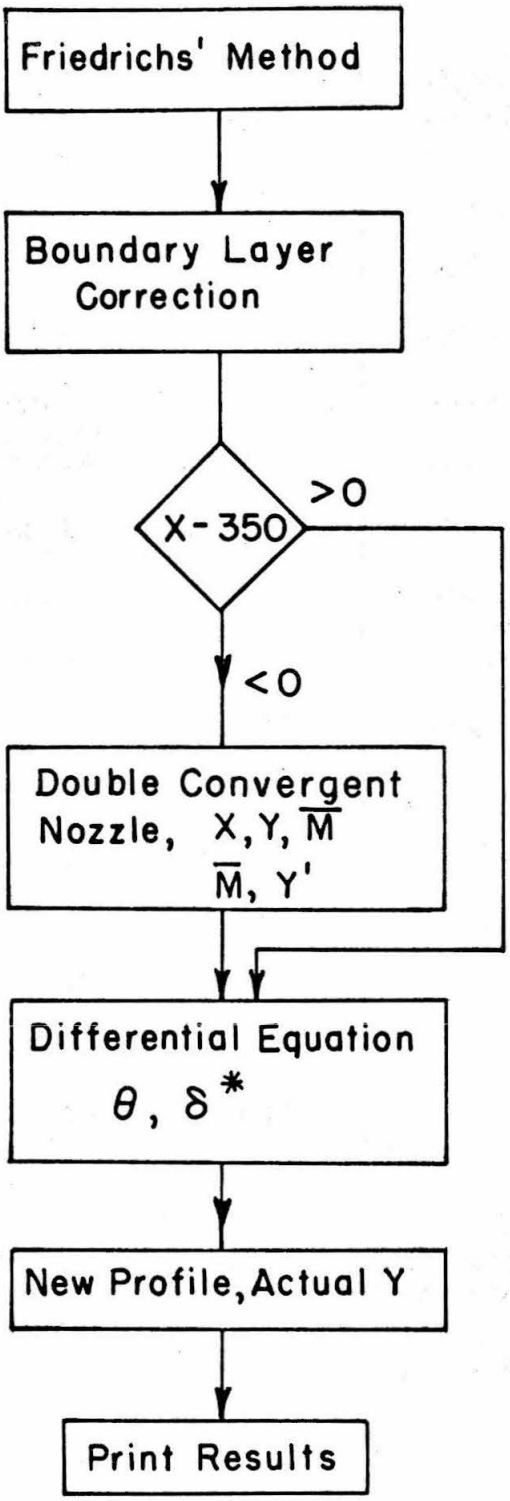

TABLE 4 COMPUTER PROGRAM USED TO DESIGN THE WHOLE NOZZLE WITH BOUNDARY LAYER CORRECTION

x_{mm}	y_{mm}	z_{mm}	S_{mm^2}	dS/dx (mm)	Mach No.
0	250	100	50,000	0	0
25	244.75	97.91	47,931	-145	0.03
50	232.72	92.47	43,041	-236	0.04
75	215.53	84.76	36,539	-275	0.04
100	195.20	75.76	29,577	-275	0.05
125	173.48	66.27	22,995	-247	0.06
150	151.82	56.98	17,304	-205	0.08
175	131.40	48.43	12,729	-160	0.11
200	113.07	41.02	9,277	-117	0.15
225	97.43	35.00	6.821	- 80.7	0.20
250	84.79	30.49	5,172	- 52.5	0.27
275	75.15	27.47	4,129	- 32	0.34
300	68.22	25.78	3,518	- 18	0.41
325	63.46	25.10	3,186	- 9.4	0.47
350	60.00	25.00	3,000	- 6	0.60

TABLE 5. Characteristics of the Double Convergent Nozzle Used for Both Streams to Mach Number 0.5 .

x_{mm}	$\bar{M}_{\#}$	$d\bar{M}/dx$ (10^{-2})	y_{mm}	dy/dx (10^{-2})
350	0.507	0.151	59.774	-12.6
375	0.540	0.166	56.685	-11.8
400	0.585	0.188	53.850	-10.7
425	0.636	0.212	51.309	- 9.5
450	0.693	0.239	49.110	- 8.0
475	0.758	0.267	47.305	- 6.4
500	0.830	0.298	45.950	- 4.5
525	0.910	0.329	45.008	- 2.4
550	0.998	0.360	44.847	-10^{-4}
575	1.094	0.389	45.237	+ 2.6
600	1.197	0.414	46.332	+ 5.4
625	1.300	0.382	47.677	+ 7.3
650	1.374	0.196	49.042	+ 4.5
675	1.398	0.026	49.594	+ 0.64
700	1.399	10^{-9}	49.967	10^{-6}
725	1.399	0	49.997	0
750	1.400	0	50.000	0

TABLE 6. Mach Number Distribution and Wall Contour for the Supersonic Nozzle before Boundary Layer Correction.

$X_{(mm)}$	$M_{\#}$	$\theta_{(mm)}$	$\delta_{*(mm)}$
0	0	0.000	0.000
50	0.04	0.2088	0.2612
100	0.05	0.1940	0.2428
150	0.08	0.1526	0.1912
200	0.15	0.1233	0.1554
250	0.27	0.1136	0.1457
300	0.41	0.1296	0.1718
350 (1)	0.50	0.1769	0.2410
400	0.58	0.2137	0.3000
450	0.69	0.2281	0.3345
500	0.83	0.2295	0.3581
550 (2)	1.00	0.2253	0.3827
600	1.20	0.2208	0.4186
650	1.37	0.2326	0.4885
700 (3)	1.40	0.2980	0.6352
750	1.40	0.3689	0.7866
800	1.40	0.4364	0.9304
850	1.40	0.5012	1.0685
900	1.40	0.5638	1.2019
950	1.40	0.6245	1.3315
1000	1.40	0.6838	1.4578
1050	1.40	0.7417	1.5812
1100	1.40	0.7984	1.7021

TABLE 7. Values of θ and δ^* for the Supersonic Stream

X(mm)	θ(mm)	δ^*(mm)
700	0.298	0.635
800	0.436	0.930
900	0.564	1.202
1000	0.684	1.458
1100	0.798	1.702
1200	0.909	1.937
1300	1.043	2.170
1400	1.152	2.470
1500	1.254	2.69
1600	1.356	2.91
1700	1.456	3.12
1800	1.570	3.36
1900	1.665	3.56

TABLE 8. Values of θ and δ^* for the Supersonic Stream and for Values of x Corresponding to the Test Section

$X_{(mm)}$	$M_{\#}$	$\theta_{(mm)}$	$\delta^*_{(mm)}$
0	0	0	0
50	0.04	0.2484	0.3107
100	0.05	0.2291	0.2867
150	0.08	0.1796	0.2250
200	0.15	0.1451	0.1850
250	0.27	0.1338	0.1716
300	0.41	0.1529	0.2026
350	0.50	0.2090	0.2848
400	0.5095	0.2848	0.4028
450	0.5400	0.3730	0.5152
500	0.5620	0.4404	0.6040
550	0.5853	0.4970	0.6978
600	0.6001	0.5487	0.7709
650	0.6362	0.5829	0.8348
700	0.6641	0.6150	0.8908
750	0.6936	0.6413	0.9405
800	0.700	0.7139	1.0498

TABLE 9. Evaluation of θ and δ^* in the Subsonic Nozzle

$X_{(mm)}$	$M_{\#}$	$\theta_{(mm)}$	$\delta^{*}_{(mm)}$
900	0.7	0.9242	1.3591
1000	0.7	1.0775	1.5844
1100	0.7	1.2251	1.8015
1200	0.7	1.3681	2.0117
1300	0.7	1.5071	2.2162
1400	0.7	1.6428	2.4158
1500	0.7	1.7756	2.6110
1600	0.7	1.9057	2.8024
1700	0.7	2.0335	2.9903
1800	0.7	2.1592	3.1751
1900	0.7	2.2830	3.3571

TABLE 10. Evaluation of θ and δ^{*} for the Subsonic Stream and for Values of x Corresponding to the Test Section.

X (mm)	Y (mm)	Mach Number
350	67.35	0.50
400	62.14	0.52
450	58.39	0.54
500	55.87	0.56
550	54.35	0.58
600	53.62	0.61
650	53.46	0.63
700	53.65	0.67
750	53.97	0.69
800	54.20	0.70

TABLE 11. Wall Contour Coordinates after Boundary Layer Correction and Mach Number Distribution for the Subsonic Two-Dimensional Nozzle

$X_{(mm)}$	$Y_{(mm)}$	Mach Number
350	60.83	0.500
400	55.09	0.585
450	50.84	0.681
500	47.32	0.830
550	46.30	1.000
600	47.94	1.198
650	50.97	1.374
700	52.51	1.400
750	53.14	1.400
800	53.72	1.400

TABLE 12. Wall Contour Coordinates after Boundary Layer Correction and Mach Number Distribution for the Supersonic Two-dimensional Nozzle

z	Δu	u (m/s) without B. L.	u(m/s) with B. L.
0 (subsonic)	1	229	220
0.25	0.7	269	257
0.5	0.42	332	313
0.75	0.12	384	360
1 (supersonic)	0	405	380
			⊛

TABLE 13. Evaluation of the Velocity Profile Without and With Boundary Layer in the Turbulent Mixing Zone

⊛ For x = 100 cm

z	$T_{(^oK)}$	ρ/ρ_o	M	M^2	$\frac{\rho u}{\rho_{o_t}}$
0	270°K	0.34	0.7	0.49	77.8
0.25	260°K	0.36	0.85	0.721	96.9
0.50	245°K	0.38	1.08	1.162	126.5
0.75	230°K	0.40	1.29	1.68	156
1.00	210°K	0.43	1.40	1.96	176.3

TABLE 14. Table Showing the Different Profiles in the Mixing Zone

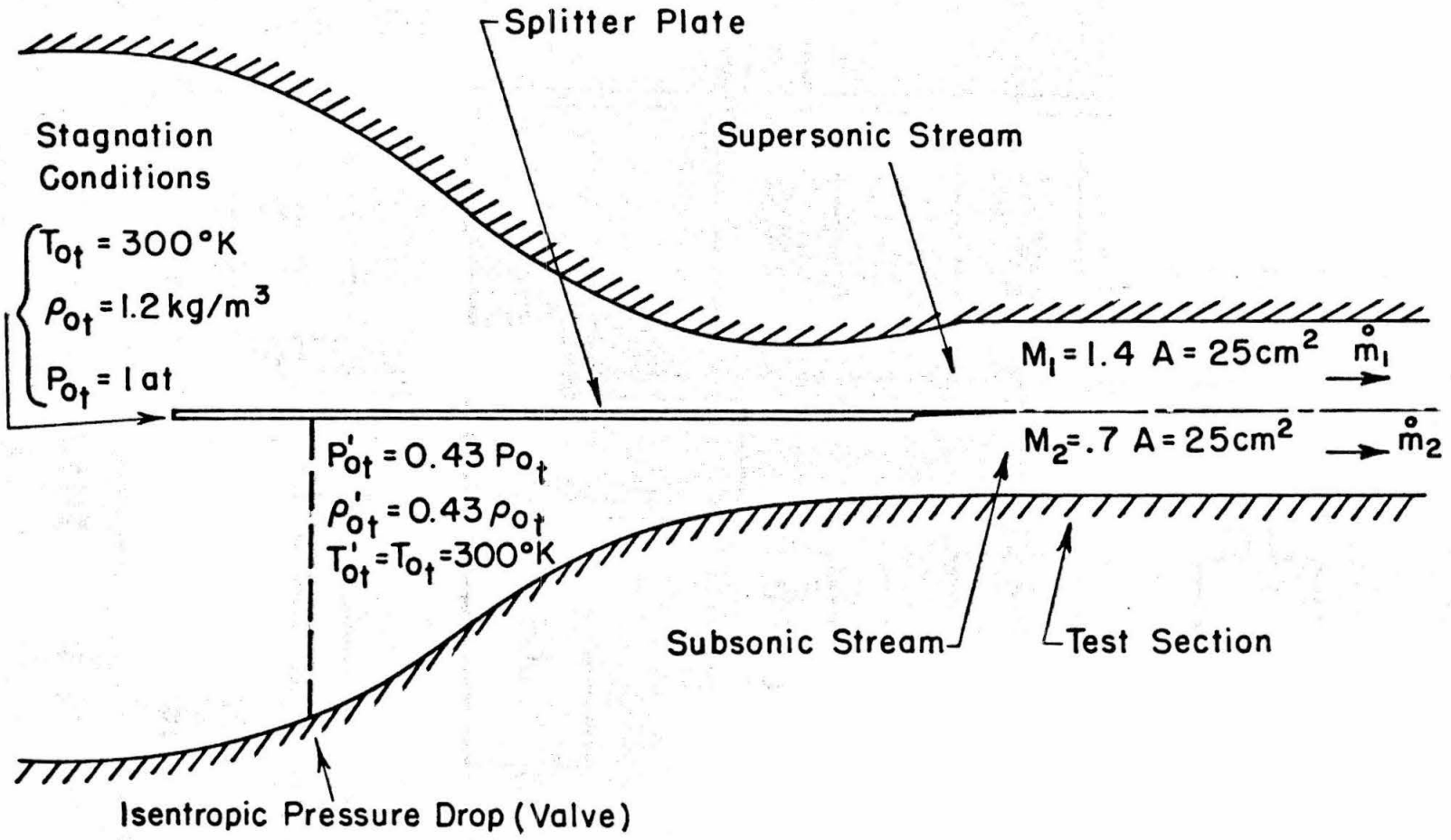

FIG. 1 FLOW CONDITIONS IN THE NOZZLE

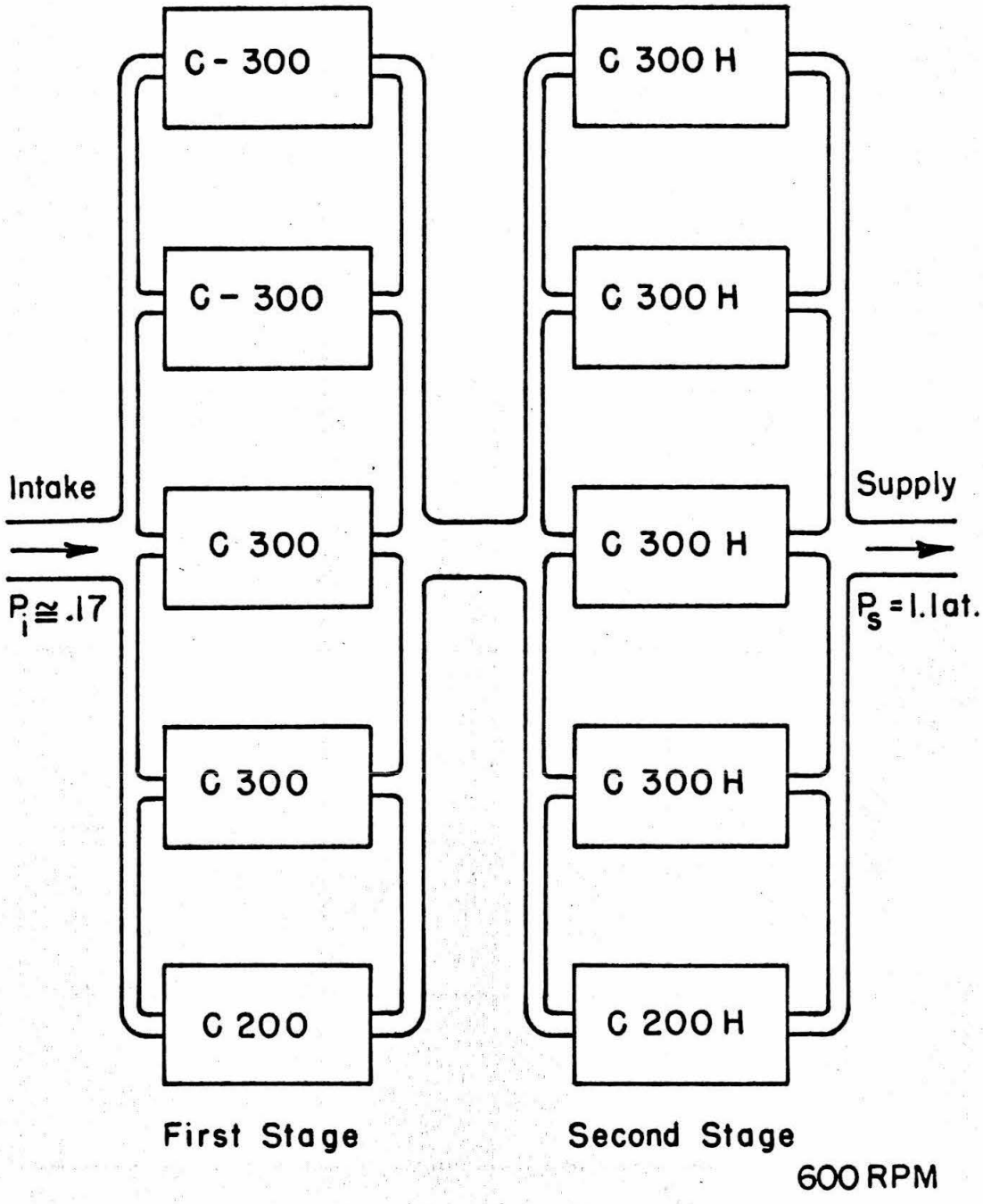

FIG. 2 COMPRESSOR PLANT STAGE ARRANGEMENTS

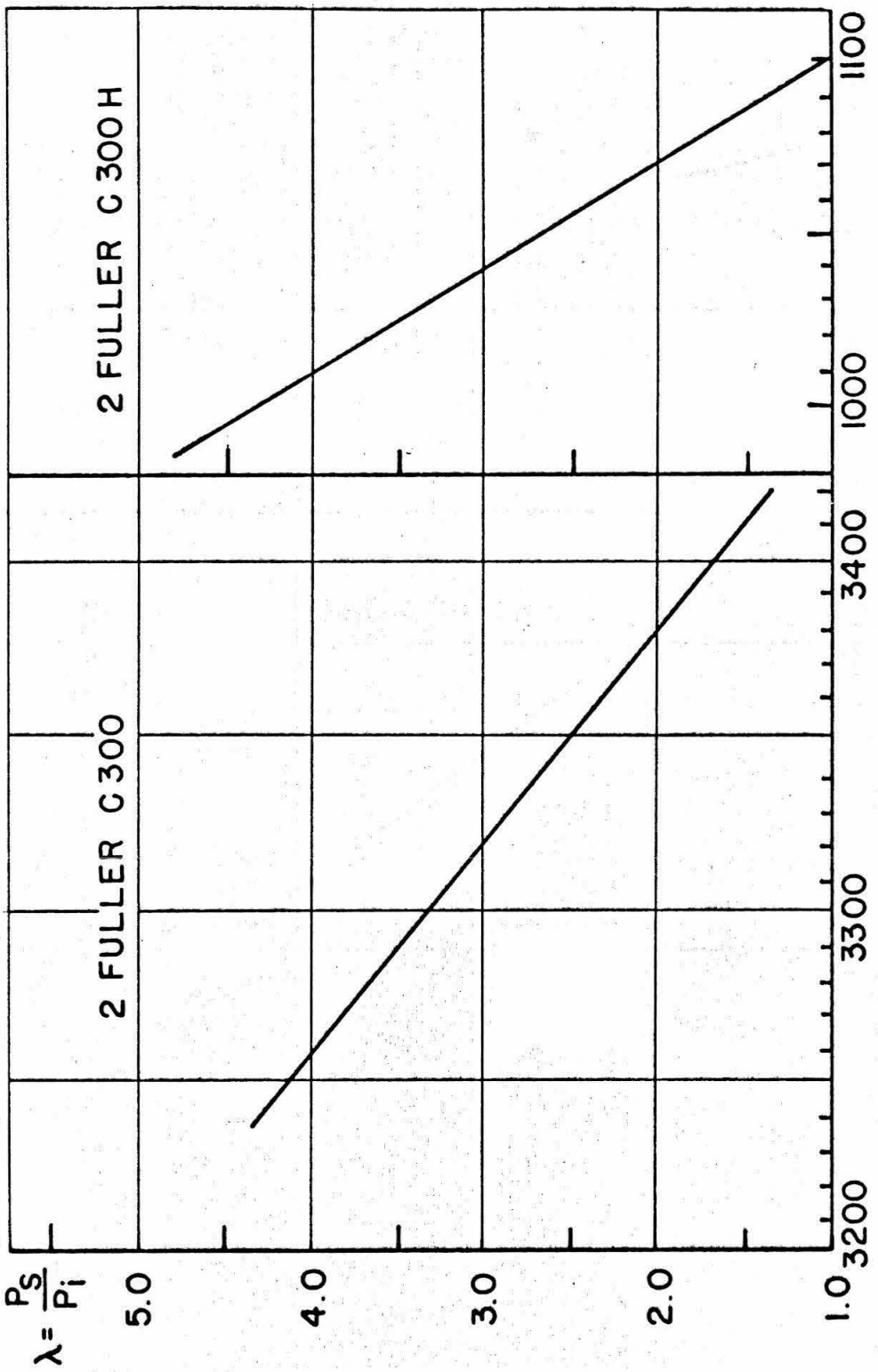

FIG. 3 CHARACTERISTIC CHART FOR THE FULLERS C 300 – C 300 H

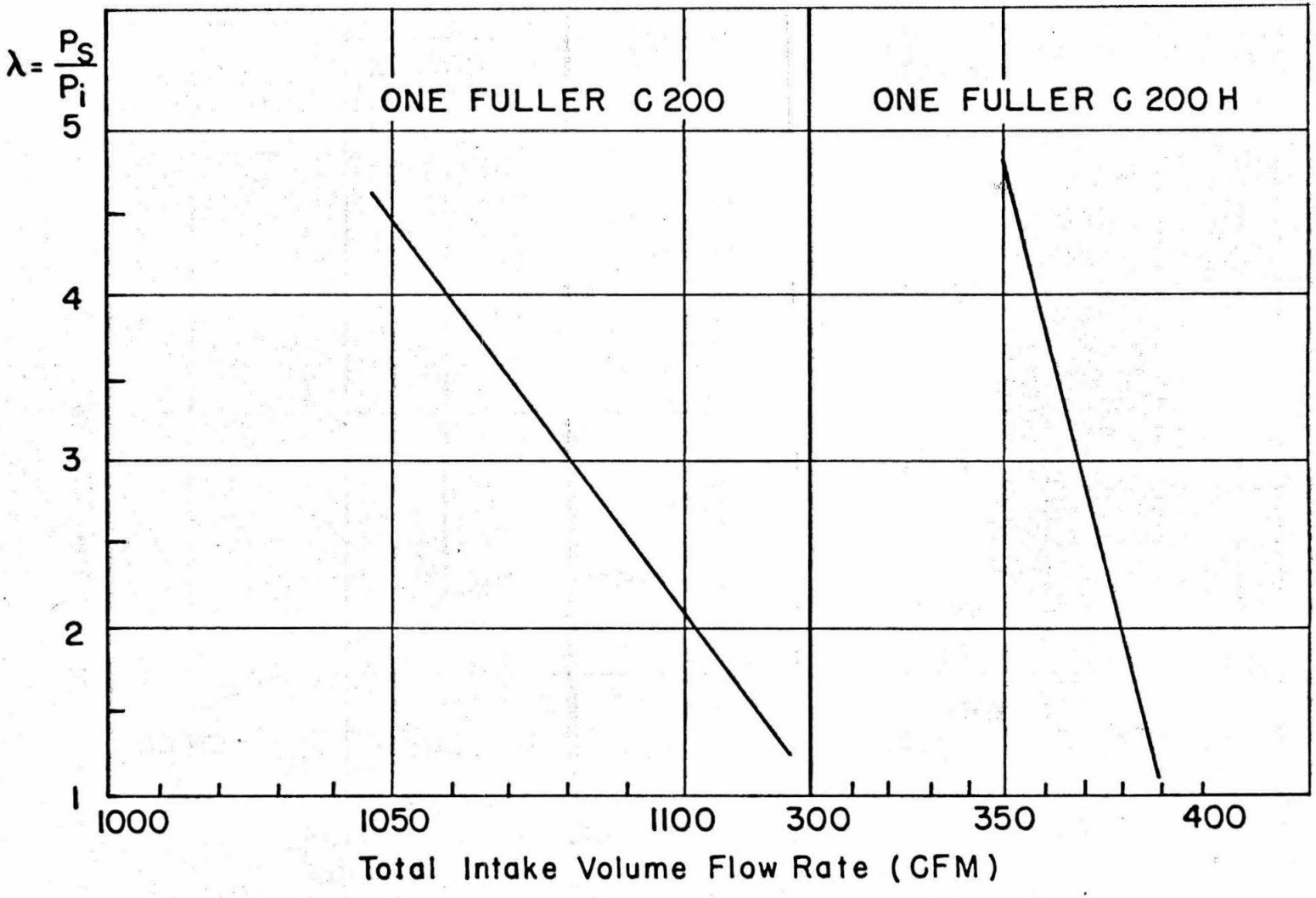

FIG. 4 CHARACTERISTIC CHART FOR THE FULLERS C200 AND C200H

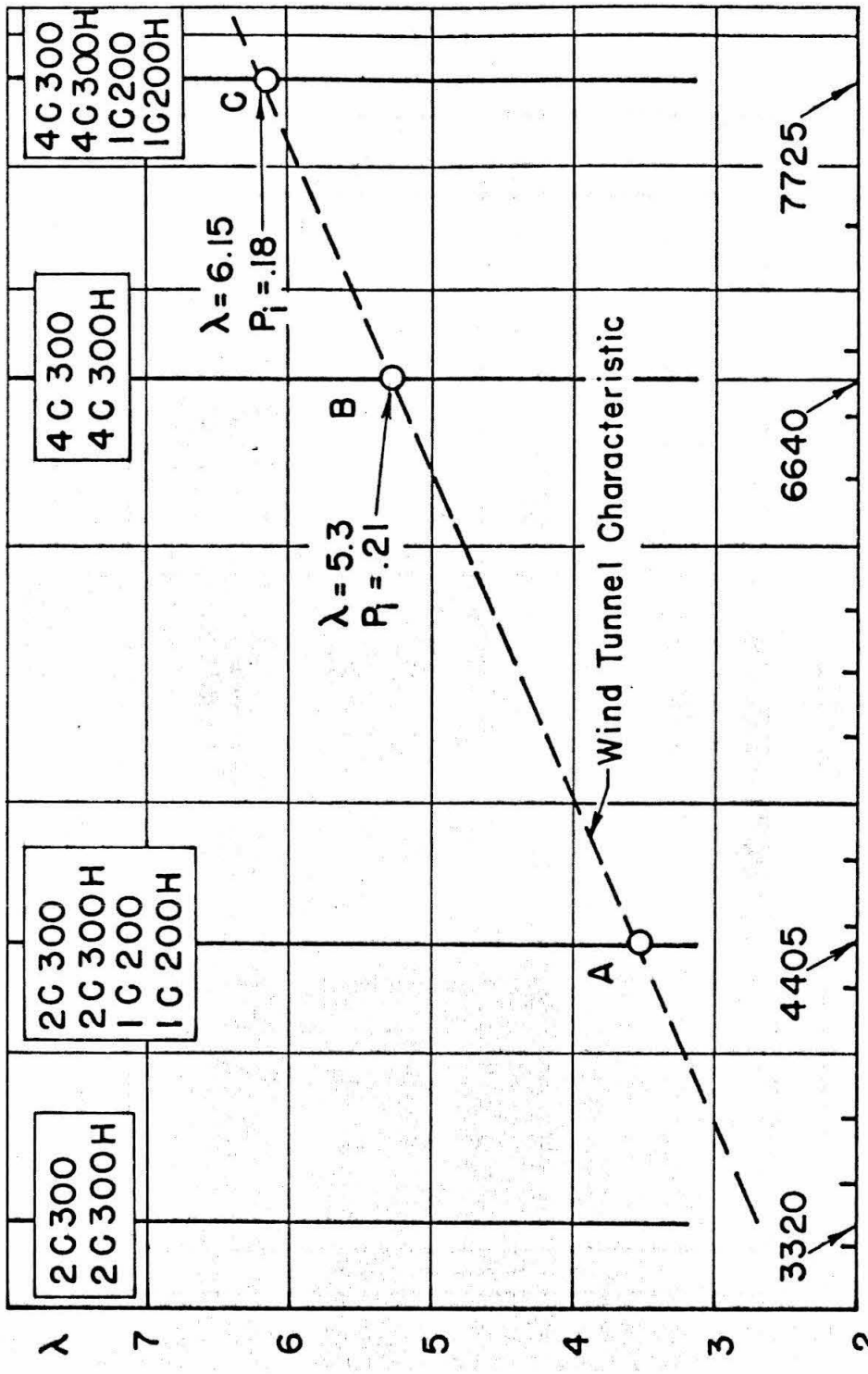

FIG. 5 MATCHING OF THE PLANT

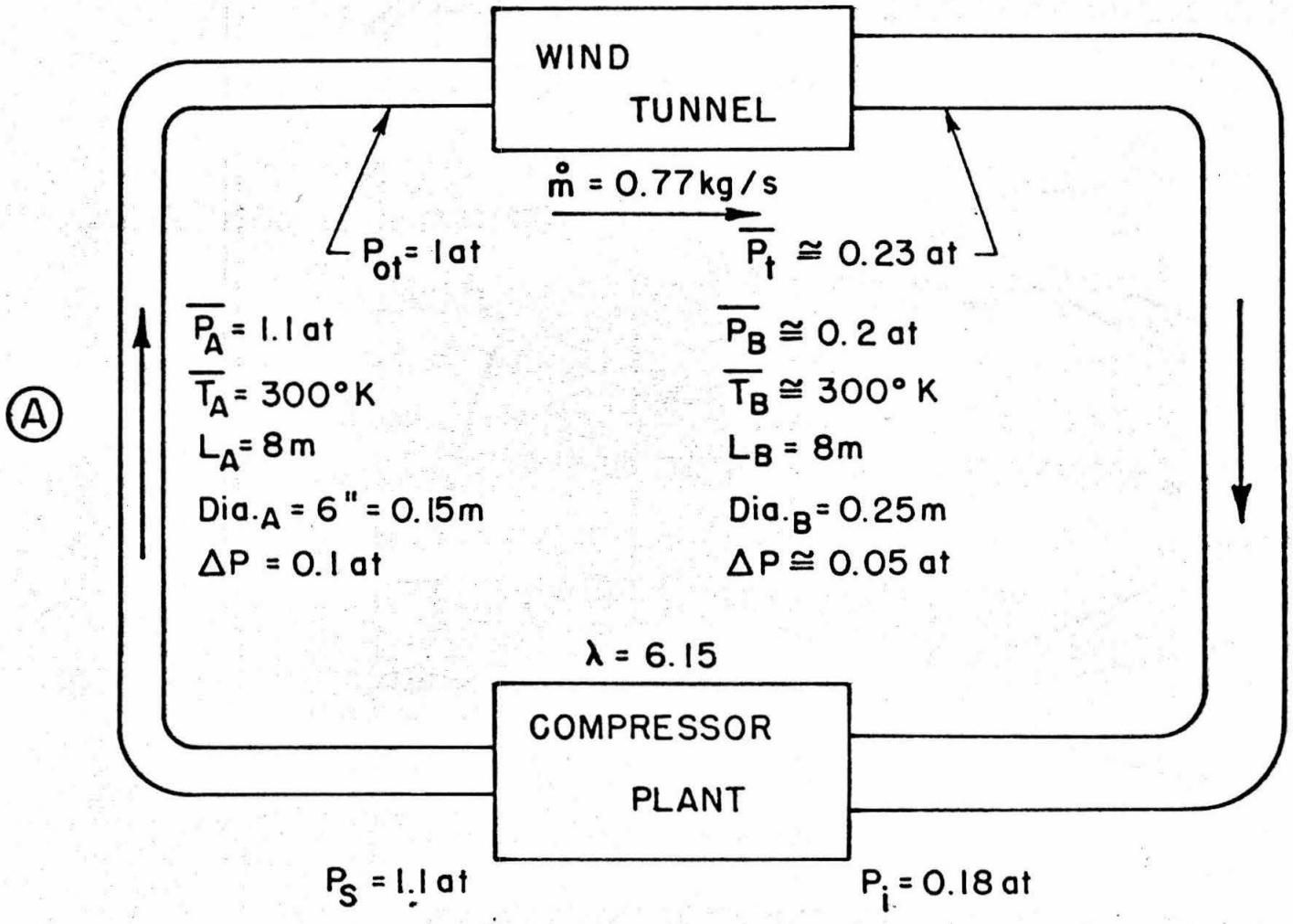

FIG. 6 ESTIMATION OF THE PRESSURES IN THE INSTALLATION

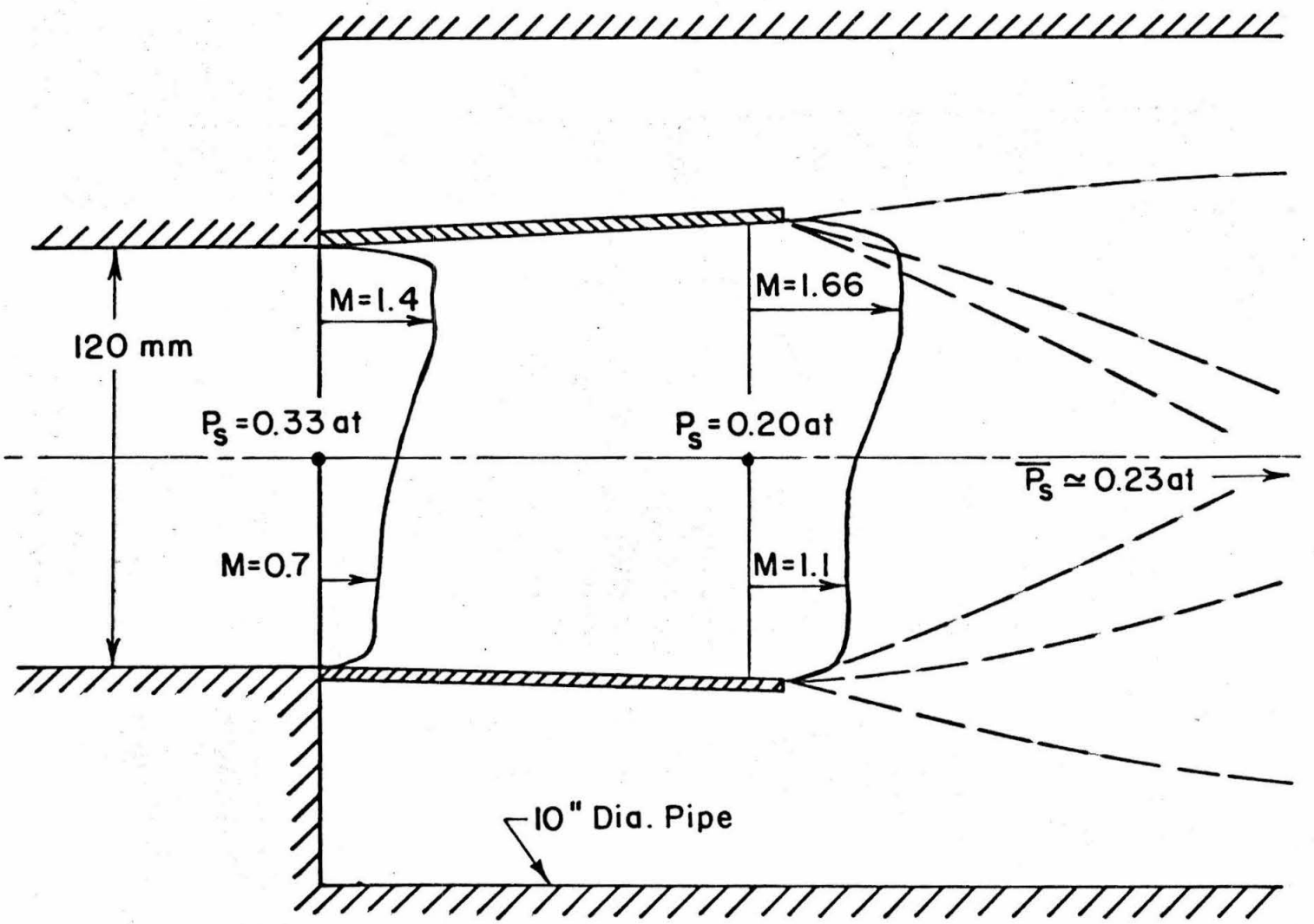

FIG. 7 MACH NUMBER DISTRIBUTION AND PRESSURES IN THE DIFFUSER

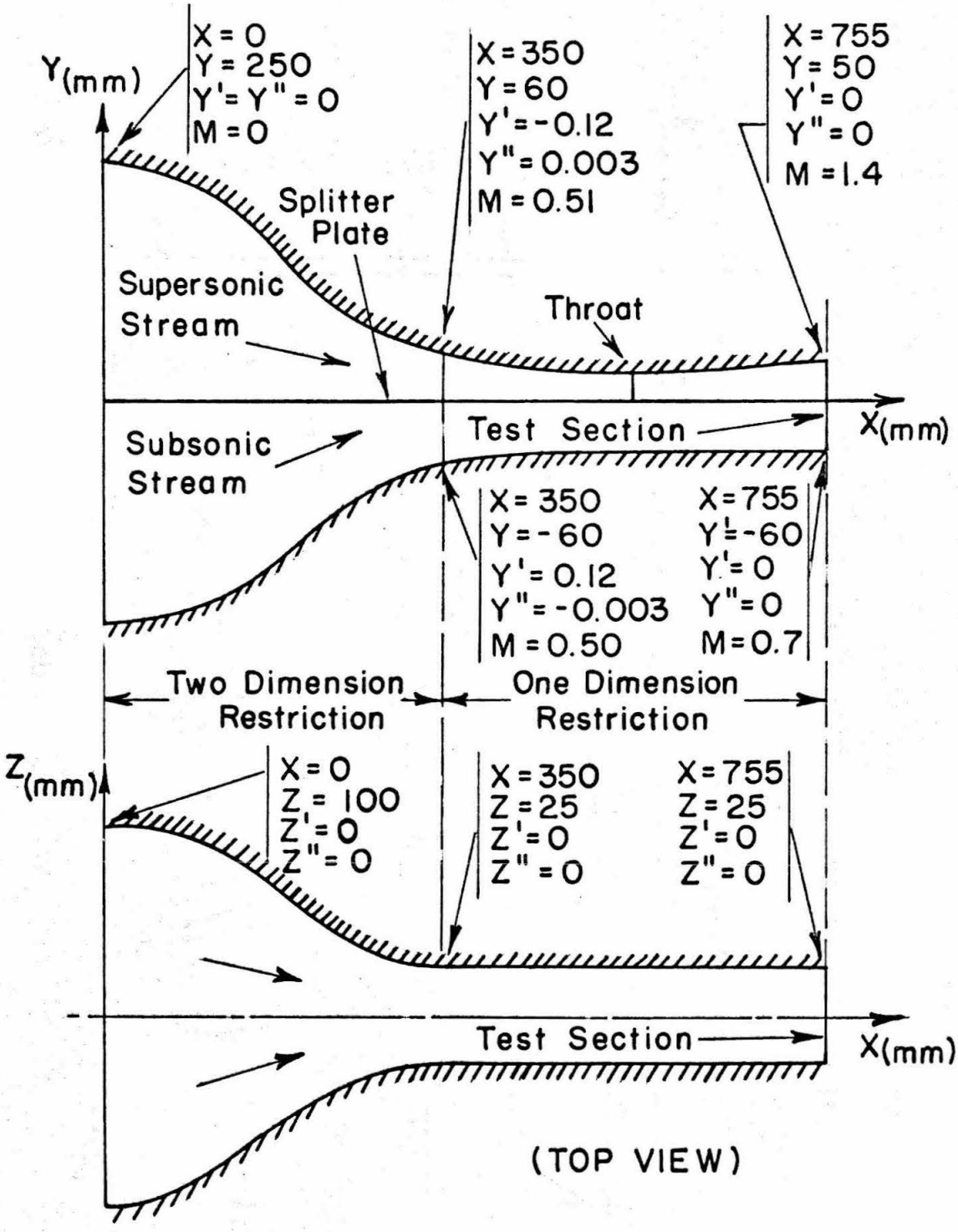

FIG. 8 GENERAL DESIGN OF THE NOZZLE BEFORE BOUNDARY LAYER CORRECTIONS

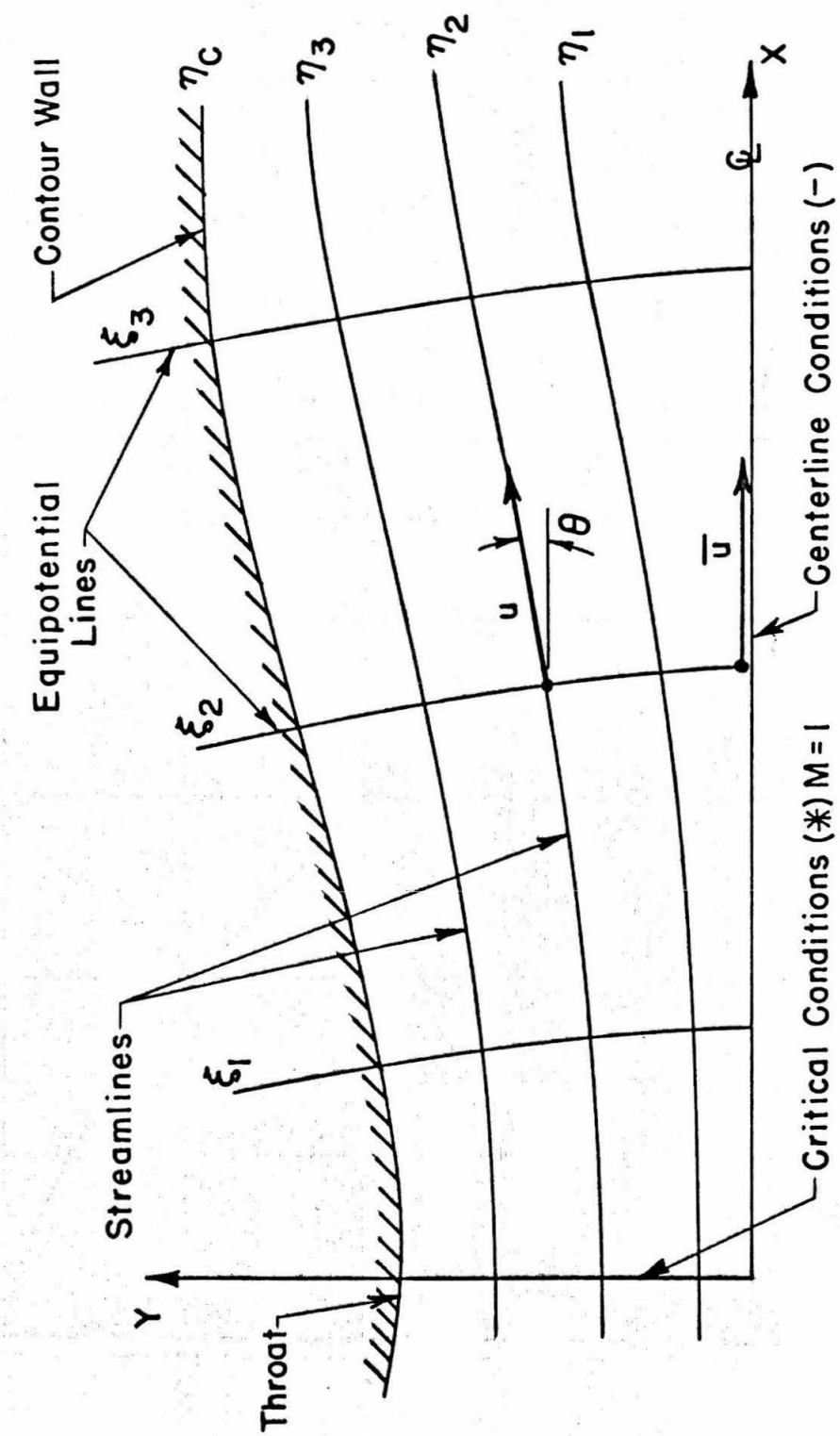

FIG. 9 COORDINATE SYSTEMS FOR FRIEDRICHS' METHOD

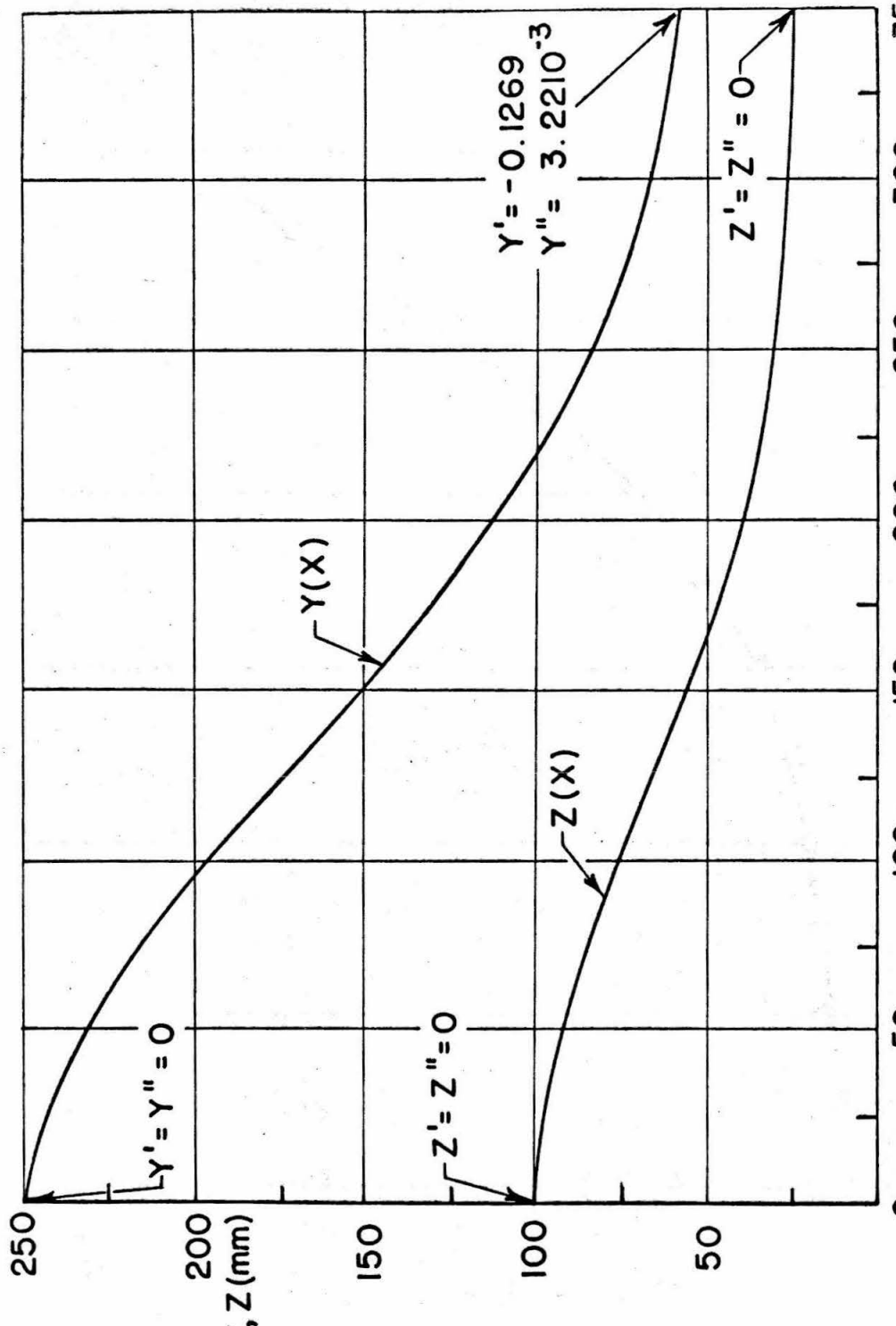

FIG. 10 DESIGN OF THE WALL CONTOURS FOR THE TWO DIMENSIONAL CONVERGENT NOZZLE (SCALE 1/2)

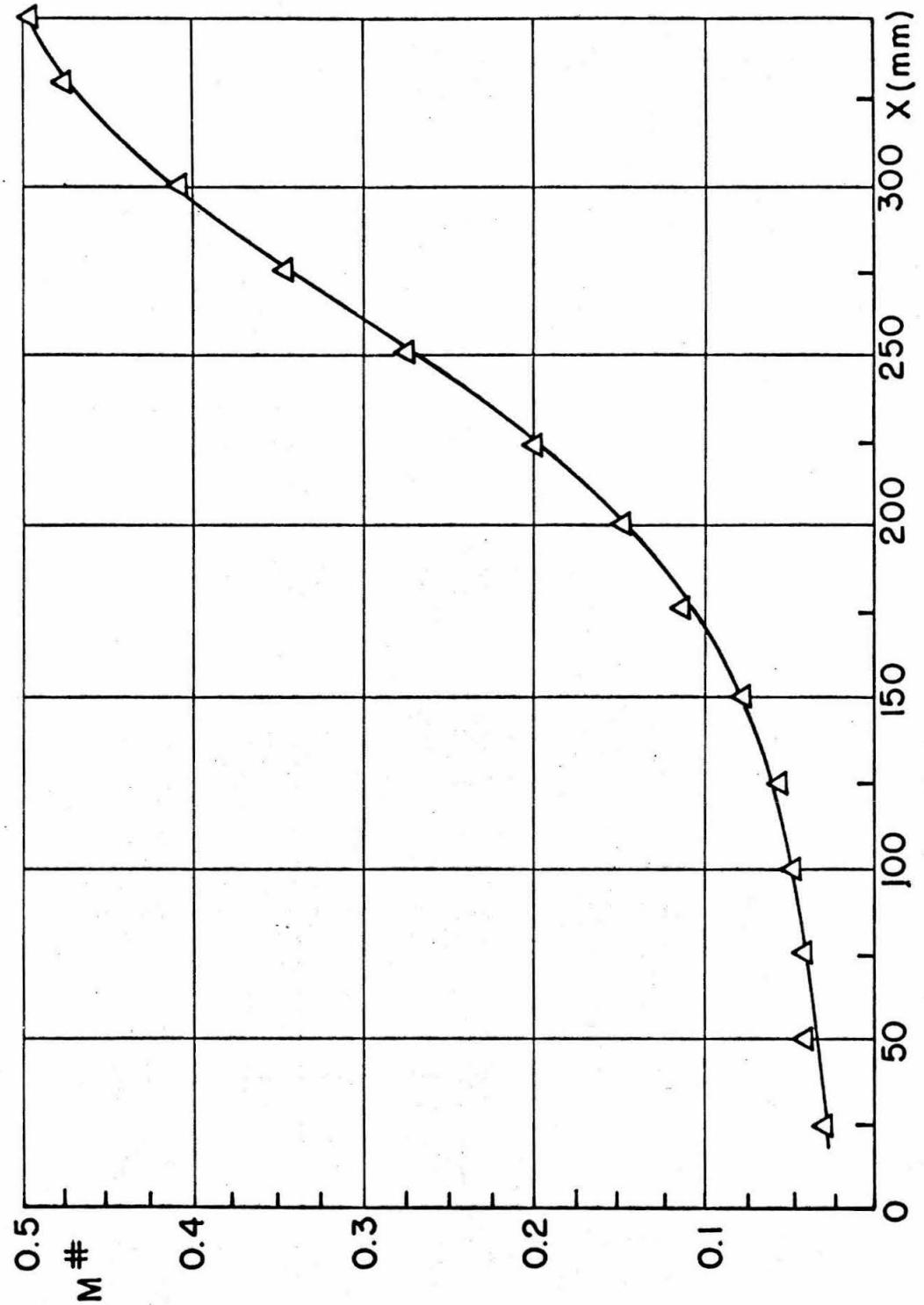

FIG. 11 MACH NUMBER DISTRIBUTION IN THE DOUBLE CONVERGENT NOZZLE

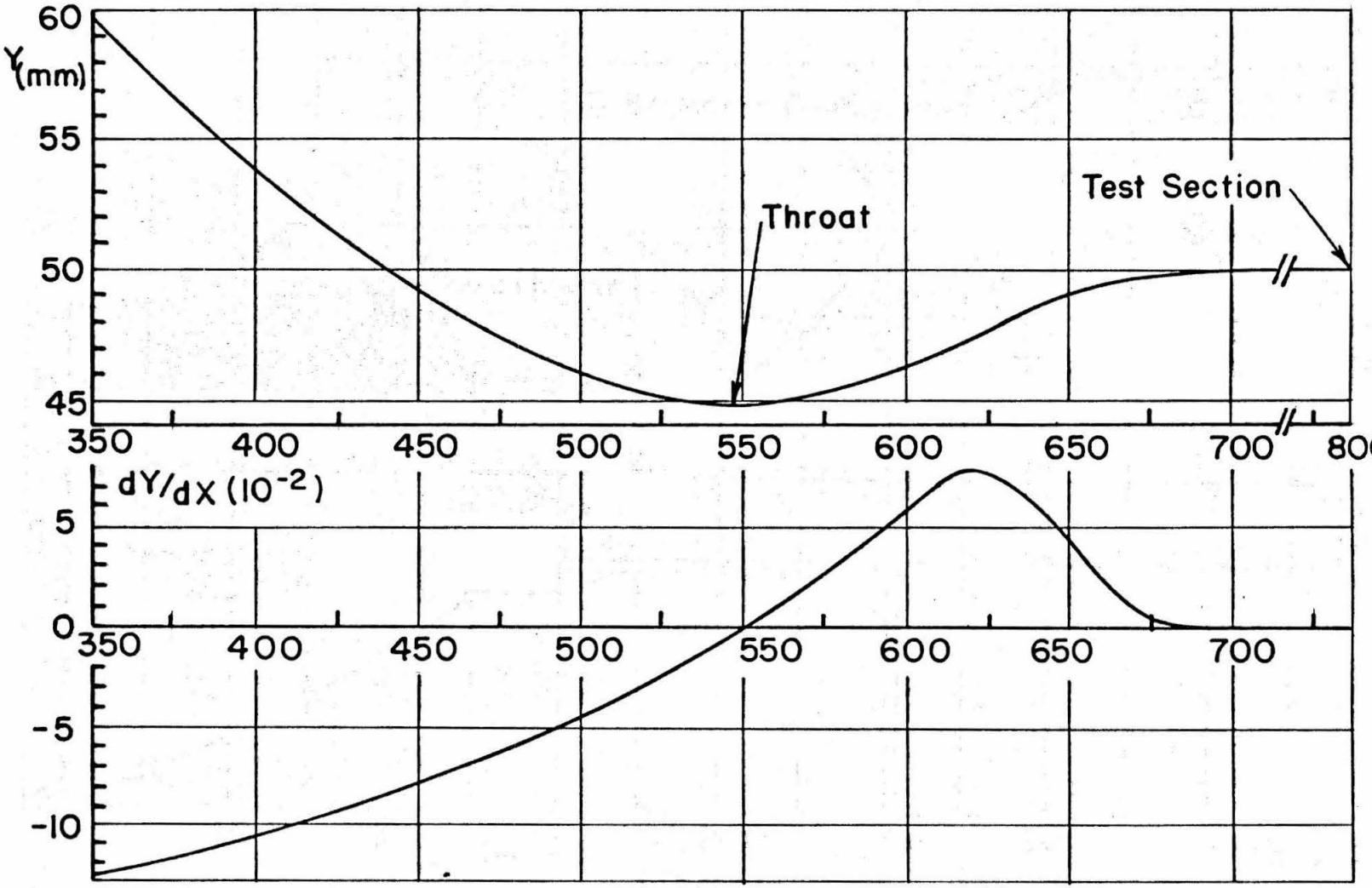

FIG. 12 WALL CONTOUR AND ITS FIRST DERIVATIVE FOR THE SUPERSONIC NOZZLE

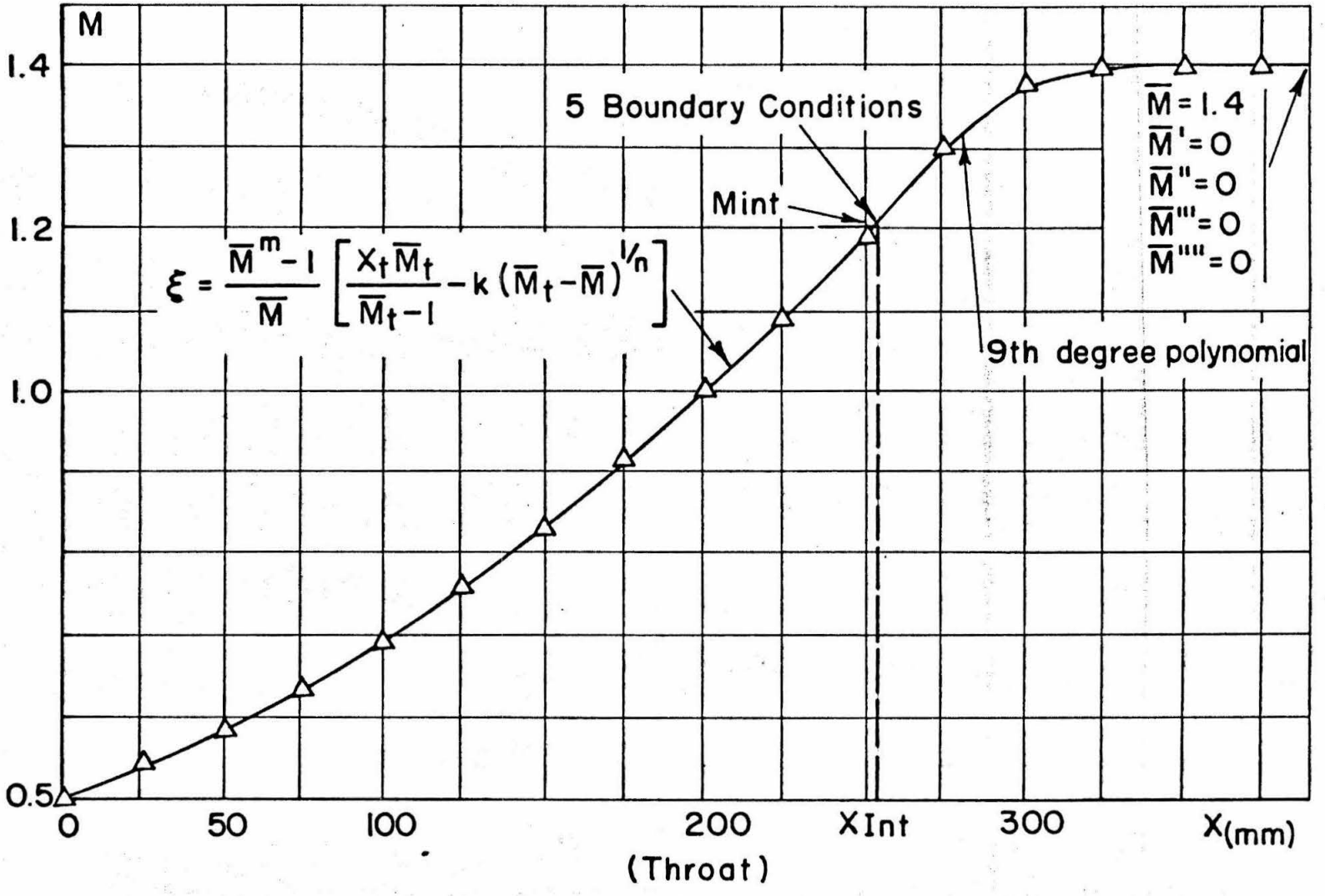

FIG. 13 MACH NUMBER DISTRIBUTION FOR THE SUPERSONIC NOZZLE

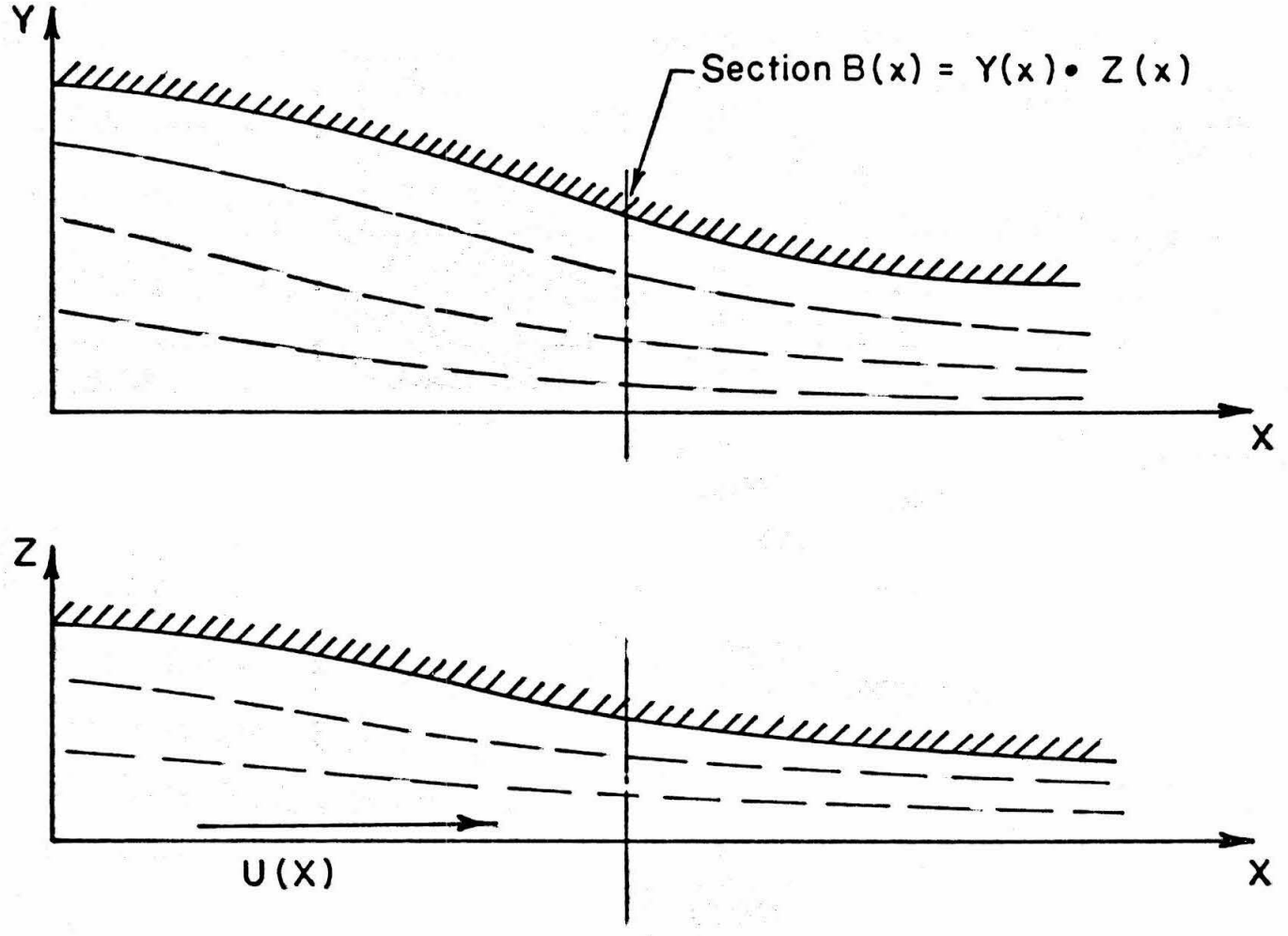

FIG.14 SYSTEM OF COORDINATES USED FOR THE BOUNDARY LAYER CALCULATION

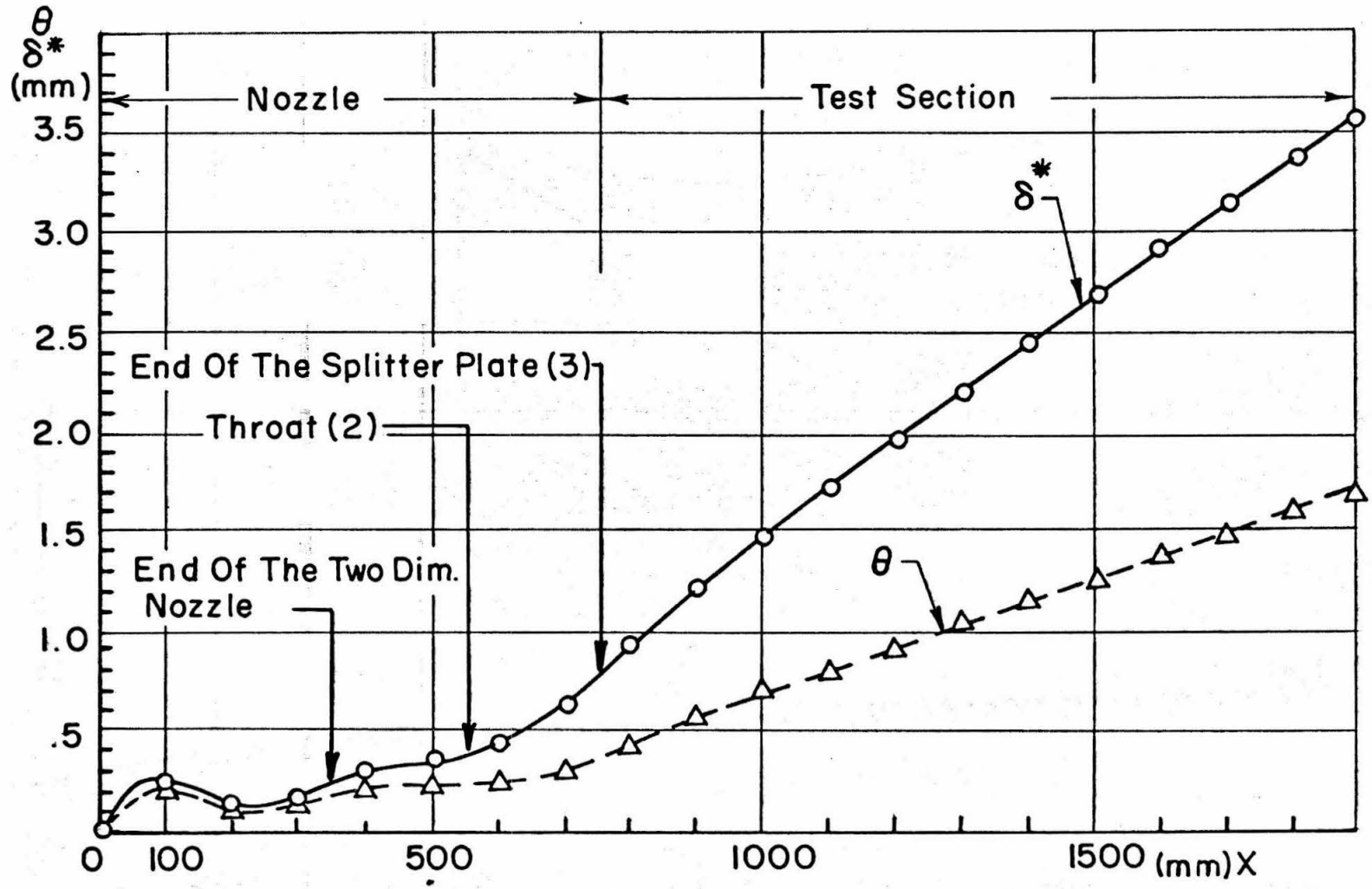

FIG. 15 VARIATION OF θ AND δ^* FOR THE SUPERSONIC STREAM

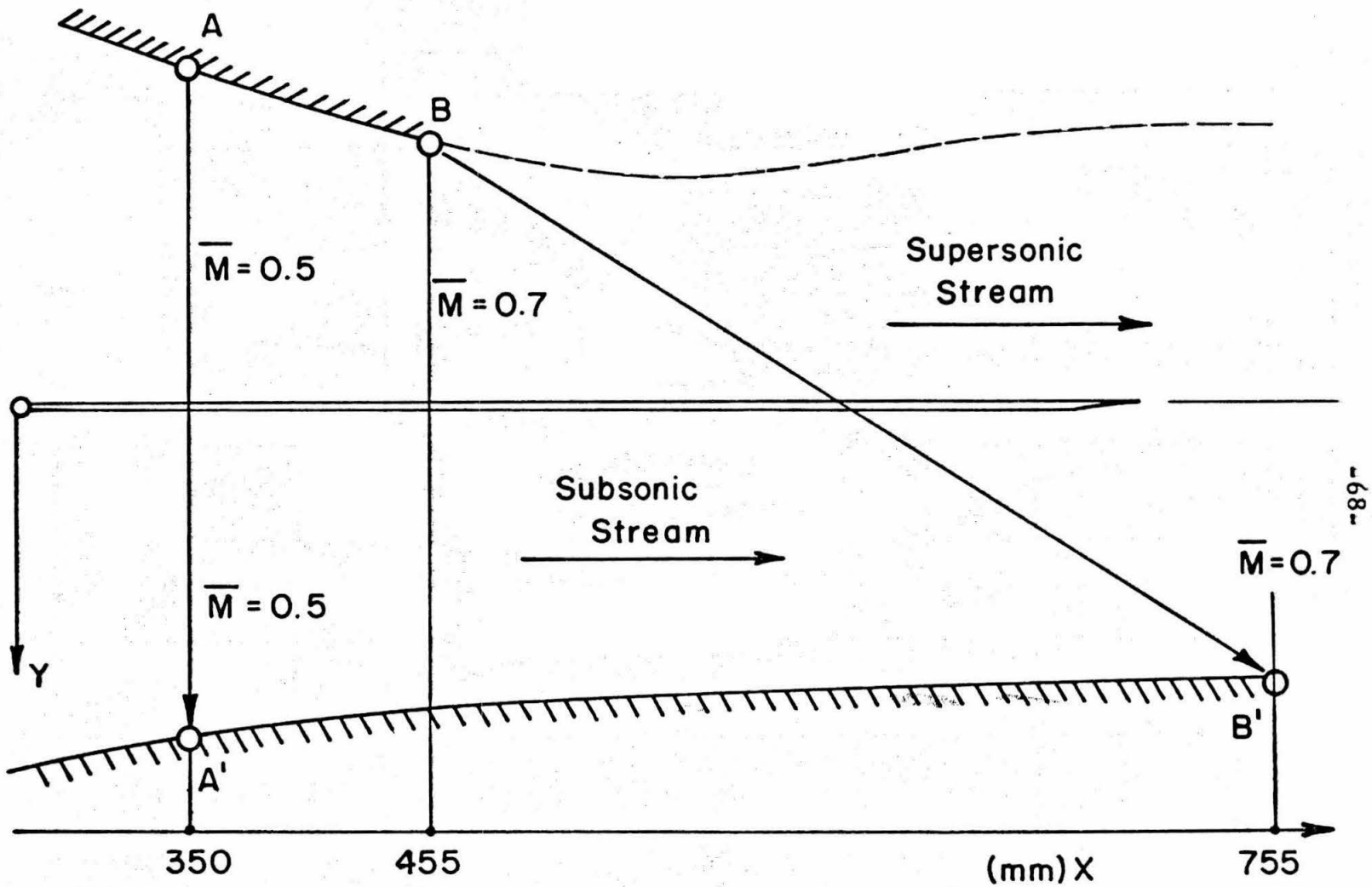

FIG. 16 TRANSFORMATION OF COORDINATES USED TO DERIVE THE SUBSONIC BOUNDARY LAYER SOLUTION

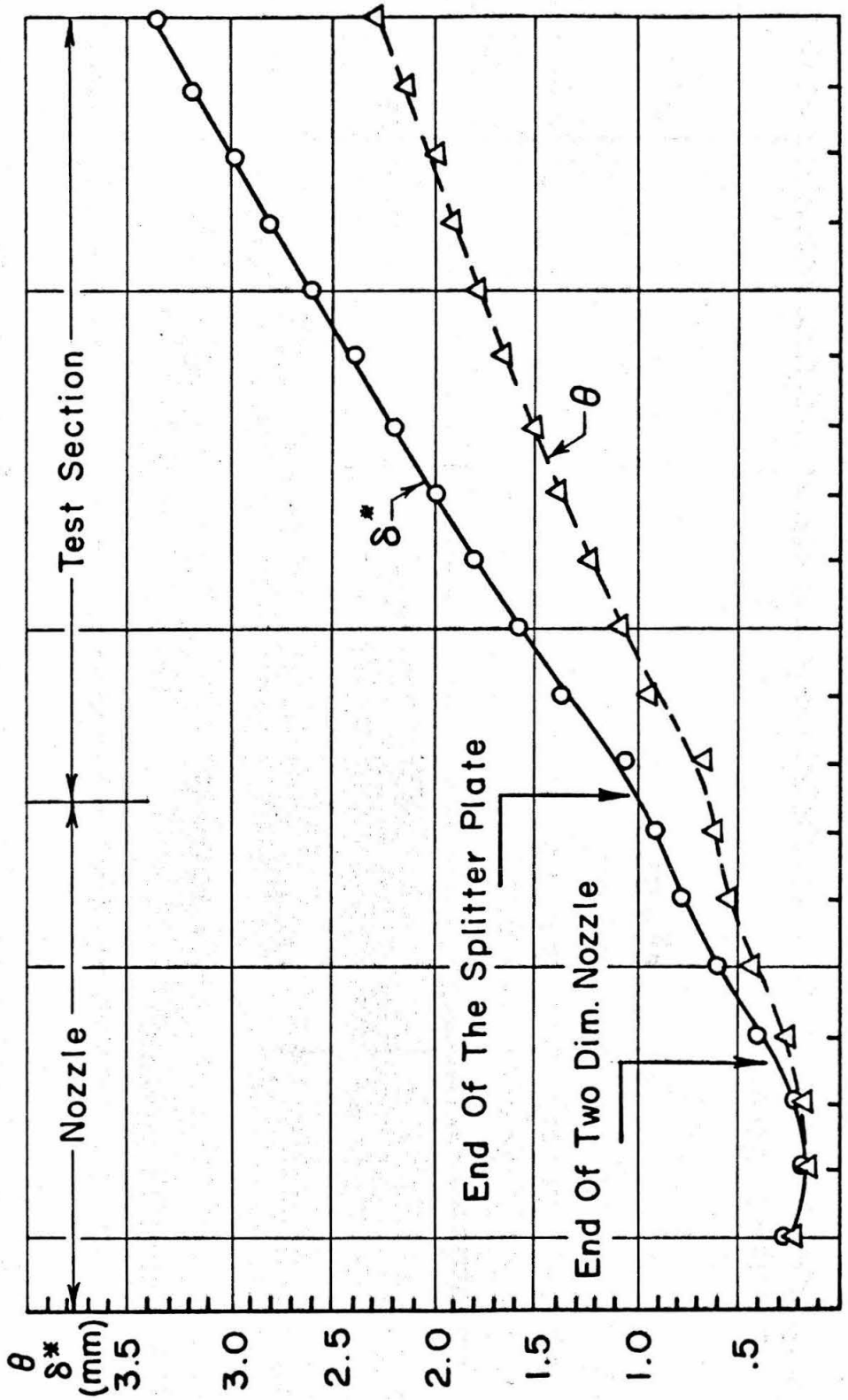

FIG.17 VARIATION OF θ AND δ^* FOR THE SUBSONIC STREAM

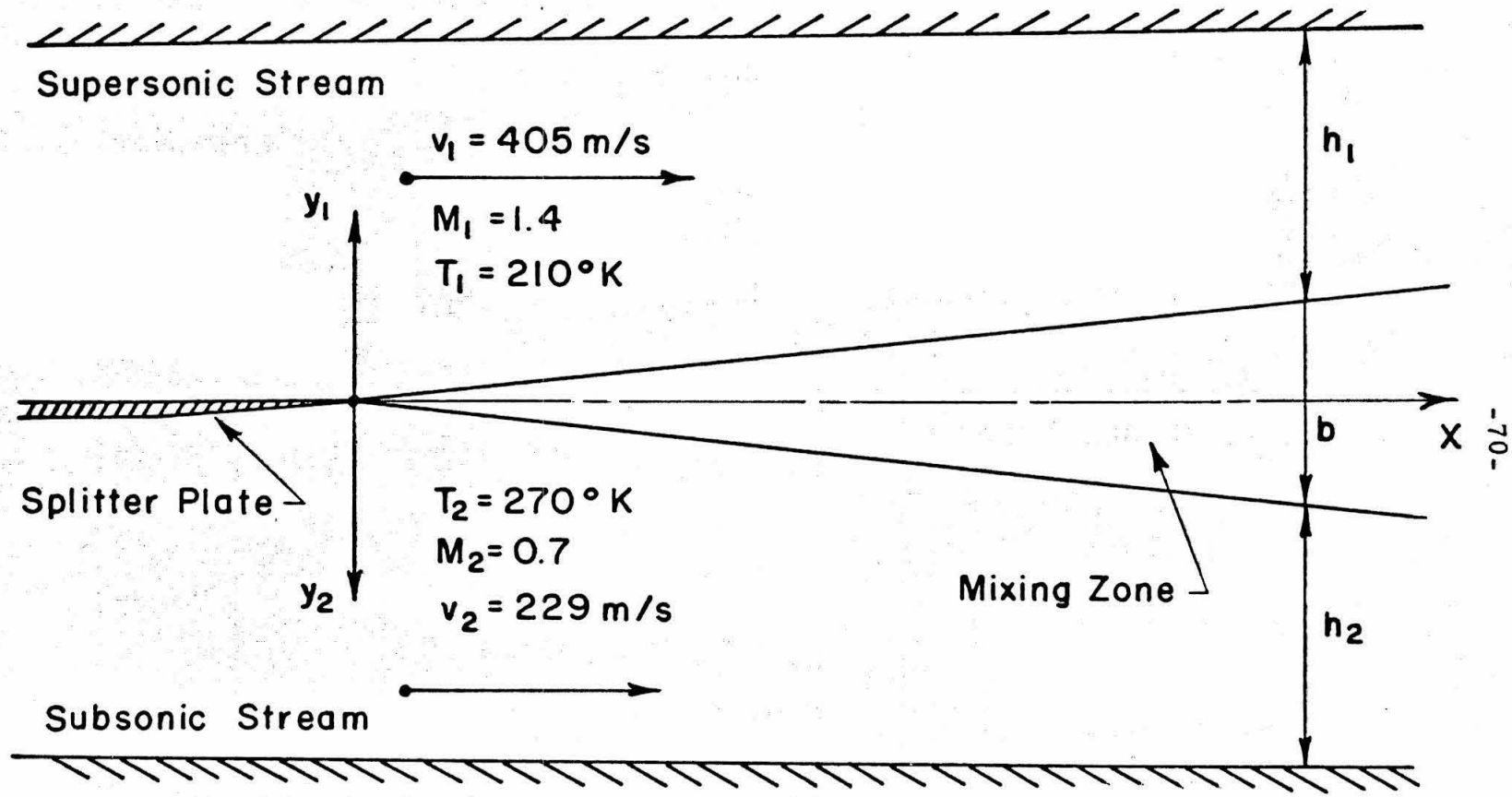

FIG. 18 CHARACTERISTICS OF THE STREAMS DOWNSTREAM OF THE SPLITTER PLATE

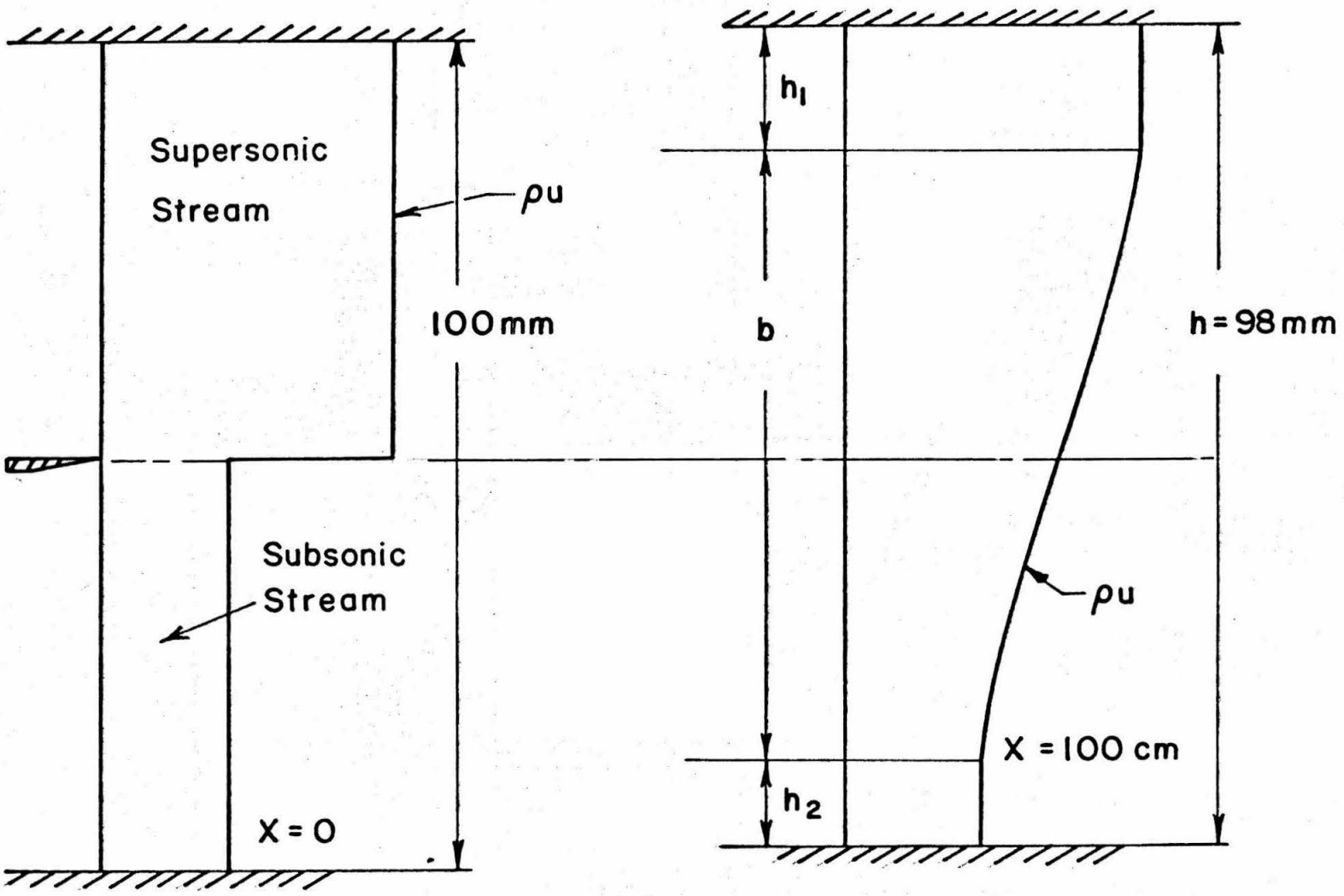

FIG. 19 ρu PROFILES AT X = 0 AND 100 cm AND DETERMINATION OF h BY INTEGRATION OF THE CONTINUITY OF MASS ALONG THE TEST SECTION

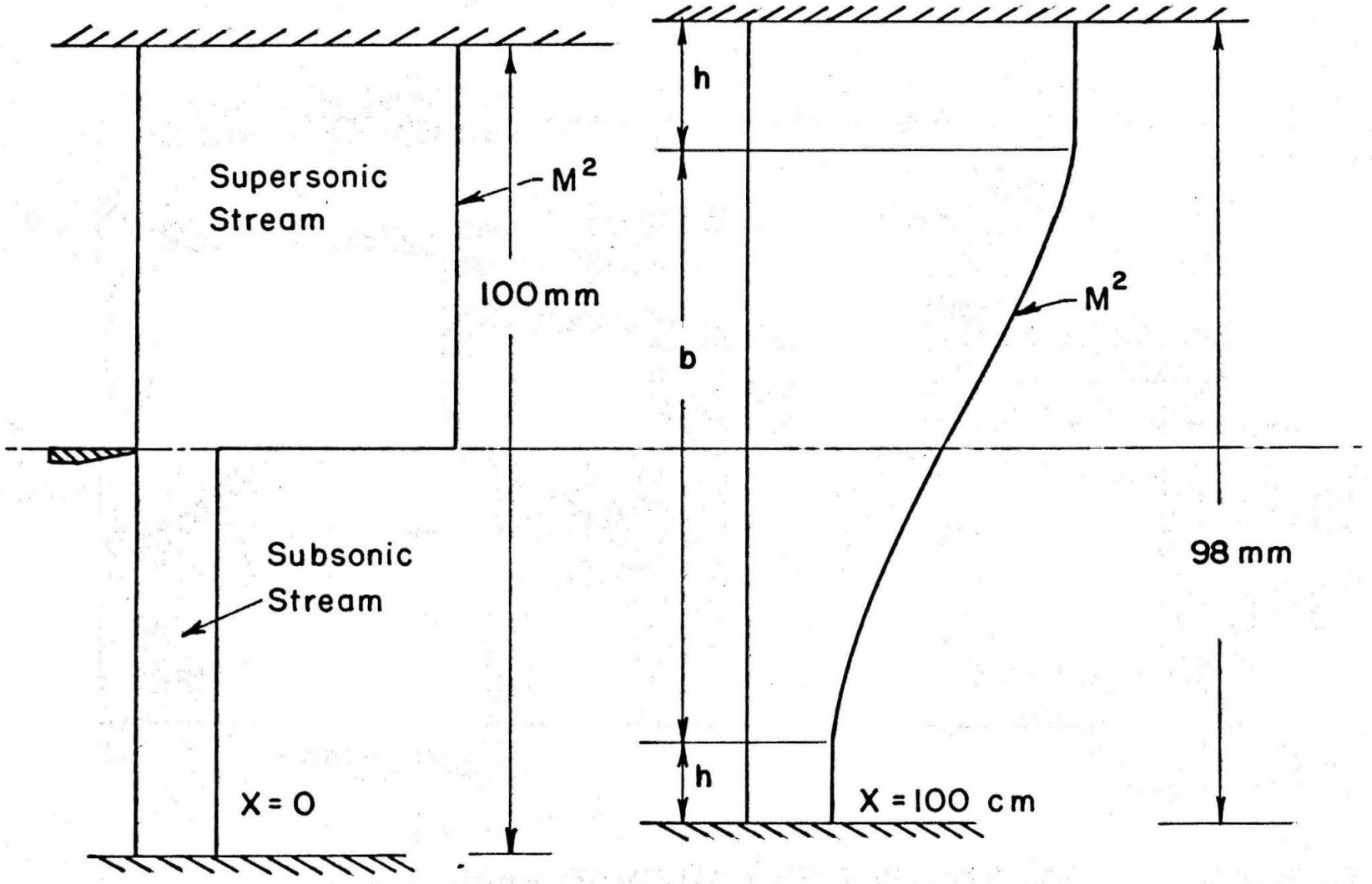

FIG. 20 M^2 PROFILES AT X = 0 AND 100cm AND DETERMINATION OF h BY INTEGRATION OF THE CONTINUITY OF X MOMENTUM ALONG THE TEST SECTION

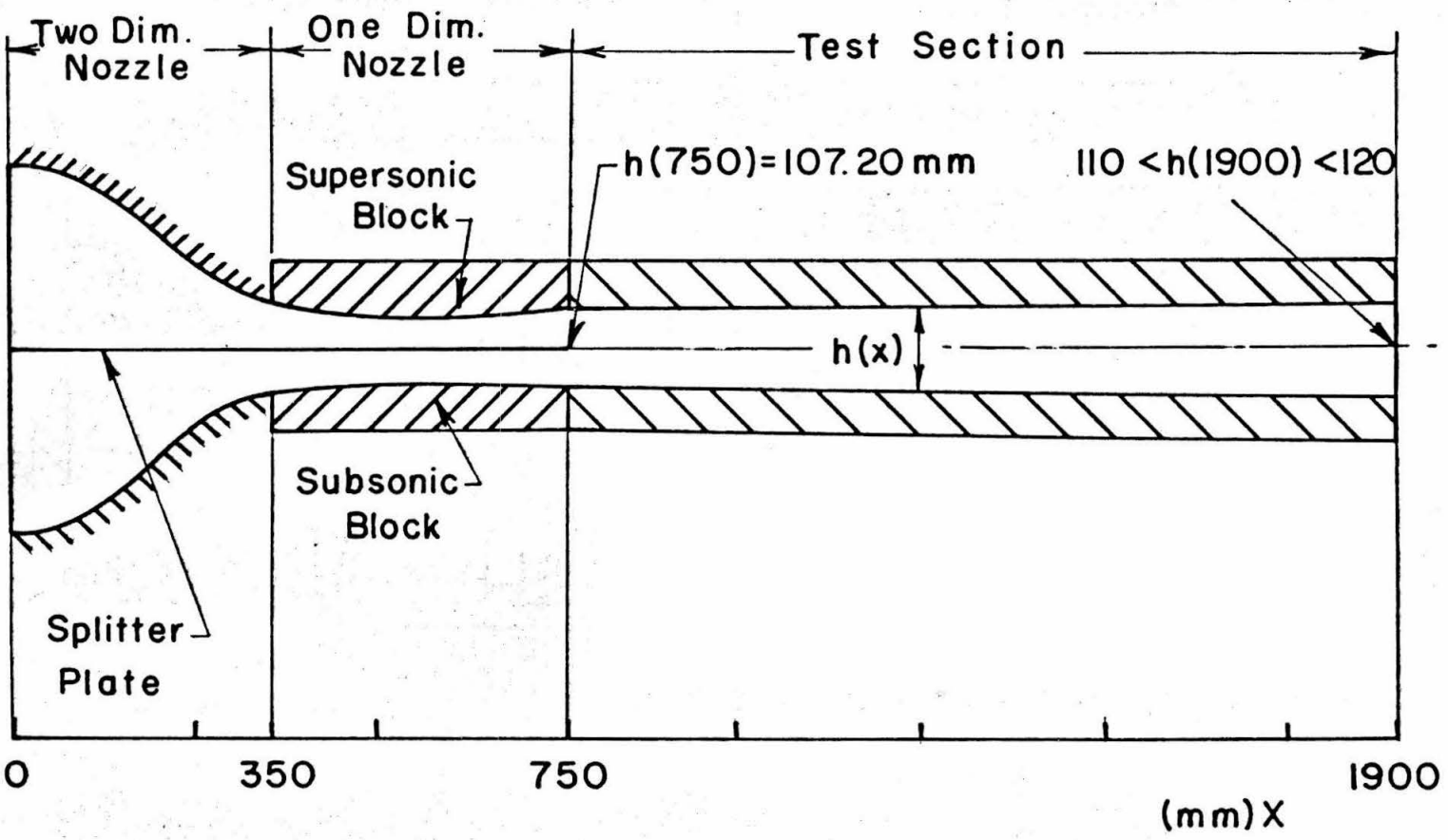

FIG. 21 GENERAL CHARACTERISTICS OF THE WIND TUNNEL (SCALE 1/10)

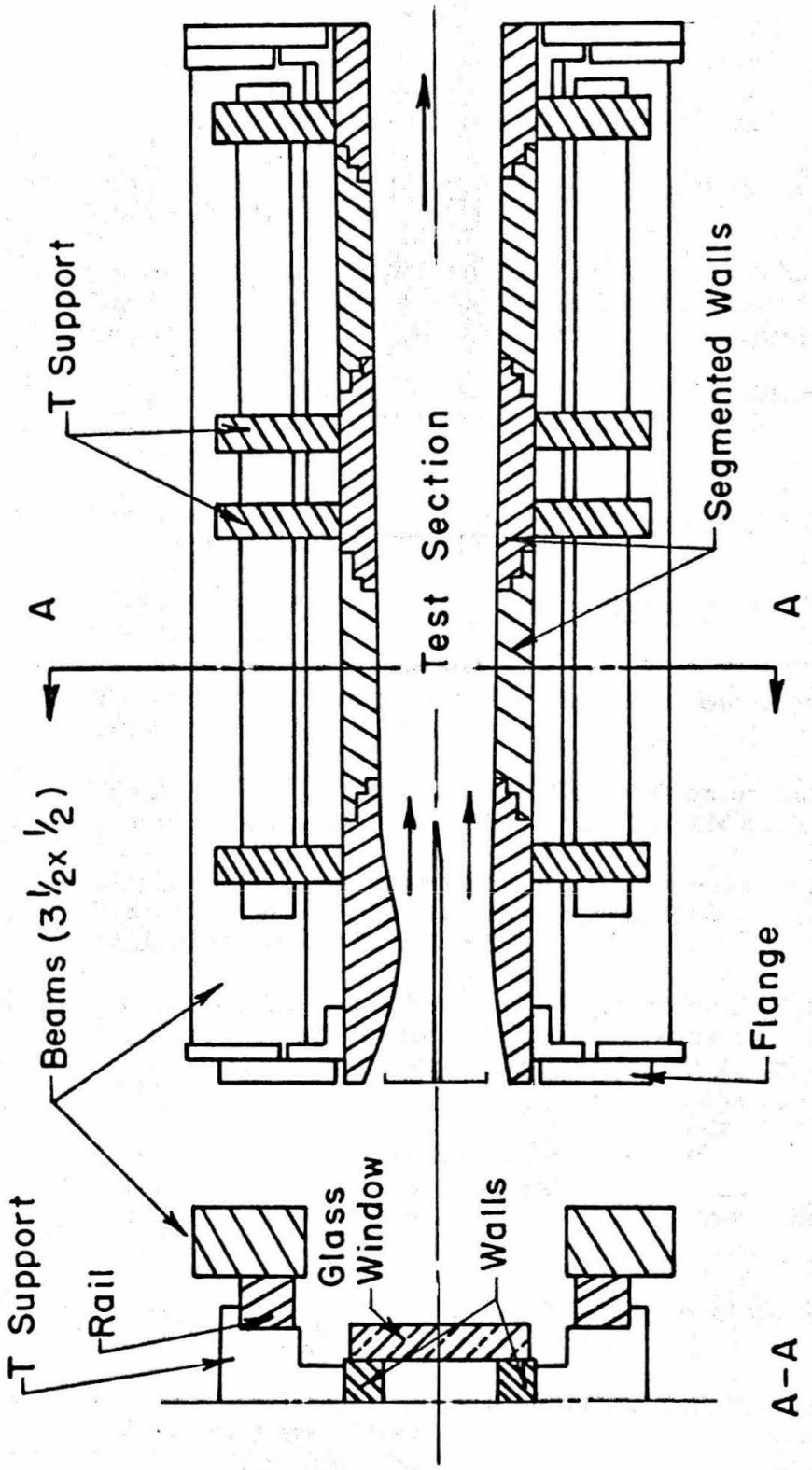

FIG. 22 STRUCTURE OF THE WIND TUNNEL

REFERENCES

1. Kubota, T., "Characteristics of Hypersonic Compressor Plant," GALCIT Hypersonic Project Internal Memorandum 3, California Institute of Technology (May 1956).

2. Ouziaux, R., Mécanique des fluides appliquée, Tome II, Dunod, Paris (1967).

3. Squires, R. K., Roberts, R. C., Fisher, E. R., "A Method for Designing Supersonic Nozzles Using the Centerline Mach Number Distribution," NAVORD Report 3995 (October 1956).

4. Nilson, E., "Design of an Inlet for a Two-dimensional Supersonic Nozzle," United Aircraft Corp., Project Meteor (December 1947).

5. Liepmann, H. W., Roshko, A., Elements of Gasdynamics, John Wiley, New York (1957).

6. Schlichting, H., Boundary Layer Theory, McGraw-Hill, New York (1968).

7. Tucker, M., "Approximate Turbulent Boundary Layer Development," NACA TN 2045 (March 1950).

8. Tucker, M., "Approximate Calculation of Turbulent Boundary Layer in Compressible Flow," NACA TN 2337 (April 1951).

9. Englert, G. W., "Estimation of Compressible Boundary Layer Growth over Insulated Surfaces with Pressure Gradients," NACA TN 4022 (June 1957).

10. Reshotko, E., Tucker, M., "Approximate Calculation of the Compressible Turbulent Boundary Layer with Heat Transfer and Arbitrary Pressure Gradient," NACA TN 4154 (December 1957).

11. Cohen, N. B., "A Method for Computing Turbulent Heat Transfer in the Presence of a Streamwise Pressure Gradient for Bodies in High-speed Flow," NASA Memorandum 1-2-59L (March 1959).

12. Winkler, E. M., Persh, J., NOL Hypersonic Tunnel No. 4, NAVORD Report 3757 (July 1954).

13. Persh, J., Lee, R., "A Method for Calculating Turbulent Boundary Layer Development in Supersonic and Hypersonic Nozzles Including the Effects of Heat Transfer," NAVORD Report 4200 (June 1956).

14. Computation of Turbulent Boundary Layers, Vol. I, AFOSR-IFP Stanford Conference (1968).

15. Coles, D. E., Hirst, D. A., Computation of Turbulent Boundary Layers, Vol. II, AFOSR-IFP Stanford Conference (1968).

16. Abramovich, G. N., The Theory of Turbulent Jets, MIT Press, Cambridge, Mass. (1963).

17. Evvard, J. C. and Marcus, L. R., "Achievement of Continuous Wall Curvature in Design of Two-dimensional Symmetrical Supersonic Nozzles," NACA TN 2616 (Jan. 1952).

APPENDIX A

Review of Some Fundamental Relations Characterizing an Isentropic Flow through a Nozzle

The equation of energy may be written considering a perfect non-viscous gas

$$\frac{u^2}{2} + C_p T = \frac{u^2}{2} + \frac{\gamma RT}{\gamma - 1} = \text{constant.}$$

Introducing the local sonic velocity $a = \sqrt{\gamma RT}$ and the critical conditions at the throat we get

$$\frac{u^2}{2} + \frac{a^2}{\gamma - 1} = \frac{(\gamma+1)u^{*2}}{2(\gamma-1)} \quad .$$

Hence,

$$\frac{\gamma+1}{2} u^{*2} - \frac{\gamma-1}{2} u^2 = a^2 = \gamma RT = \gamma \frac{p}{\rho} = \gamma \frac{p^*}{\rho^*} \left(\frac{\rho}{\rho^*}\right)^{\gamma-1} = u^{*2} \left(\frac{\rho}{\rho^*}\right)^{\gamma-1} ,$$

so

$$\frac{\rho}{\rho^*} = \left[\frac{\gamma+1}{2} - \frac{\gamma-1}{2} \left(\frac{u}{u^*}\right)^2 \right]^{\frac{1}{\gamma-1}} ,$$

but because of the one-dimensional analysis

$$h = \frac{A}{A^*} = \frac{\rho^* u^*}{\rho u} = \frac{u^*}{u} \left[\frac{\gamma+1}{2} - \frac{\gamma-1}{2} \left(\frac{u}{u^*}\right)^2 \right]^{-\frac{1}{\gamma-1}} \quad .$$

Applying this relation for the centerline we get

$$\bar{h} = \frac{u^*}{\bar{u}} \left[\frac{\gamma+1}{2} - \frac{\gamma-1}{2} \left(\frac{\bar{u}}{u^*}\right)^2 \right]^{-1/(\gamma-1)} \quad .$$

Hence,

$$\frac{h}{\bar{h}} = \frac{\bar{u}}{u} \left(\frac{\frac{\gamma+1}{2} - \frac{\gamma-1}{2} \left(\frac{\bar{u}}{u^*}\right)^2}{\frac{\gamma+1}{2} - \frac{\gamma-1}{2} \left(\frac{u}{u^*}\right)^2} \right)^{\frac{1}{\gamma-1}} \quad .$$

Rewriting the energy equation for the centerline:

$$\frac{\bar{u}^2}{2} + \frac{a^2}{\gamma - 1} = \frac{\gamma + 1}{2(\gamma - 1)} u^{*2} ,$$

so

$$(\gamma - 1)\bar{u}^2 + 2a^2 = (\gamma + 1)u^{*2}$$

and

$$a^2 = \frac{(\gamma + 1)u^{*2} - (\gamma - 1)\bar{u}^2}{2} .$$

But $\bar{M}^2 = \bar{u}^2/a^2$, so

$$\bar{M}^2 = \frac{2\bar{u}^2}{(\gamma + 1)u^{*2} - (\gamma - 1)\bar{u}^2} .$$

APPENDIX B

From Appendix A we get, for the area ratio as a function of the centerline Mach number distribution,

$$\bar{h} = \frac{1}{\bar{M}}\left[\frac{(\gamma-1)\bar{M}^2+2}{\gamma+1}\right]^{\frac{\gamma+1}{2(\gamma-1)}},$$

and for the derivatives we have

$$\bar{h}'\bar{M}[(\gamma-1)\bar{M}^2+2] = 2\bar{h}\bar{M}'(\bar{M}^2-1)$$

$$\bar{h}''\bar{M}[(\gamma-1)\bar{M}^2+2] = 2\bar{h}\bar{M}'(\bar{M}^2-1)+4\bar{h}\bar{M}'^2\bar{M}-\bar{h}'\bar{M}'[(3\gamma-5)\bar{M}^2+4]$$

$$\bar{h}'''\bar{M}[(\gamma-1)\bar{M}^2+2] = 2\bar{h}\bar{M}'''(\bar{M}^2-1)+12\bar{h}\bar{M}'\bar{M}''\bar{M}+4\bar{h}\bar{M}'^3-\bar{h}''\bar{M}'[(6\gamma-8)\bar{M}^2+6]$$
$$-\bar{h}'\bar{M}''[(3\gamma-7)\bar{M}^2+6]-(6\gamma-14)\bar{h}'\bar{M}'^2\bar{M}$$

$$\bar{h}''''\bar{M}[(\gamma-1)\bar{M}^2+2] = 2\bar{h}\bar{M}''''(\bar{M}^2-1)+16\bar{h}\bar{M}'\bar{M}'''\bar{M}+12\bar{h}\bar{M}''^2\bar{M}+24\bar{h}\bar{M}'^2\bar{M}''$$
$$-\bar{h}'''\bar{M}'[(9\gamma-11)\bar{M}^2+8]-\bar{h}''\bar{M}''[(9\gamma-15)\bar{M}^2+12]$$
$$-(18\gamma-30)\bar{h}''\bar{M}'^2\bar{M}-\bar{h}'\bar{M}'''[(3\gamma-9)\bar{M}^2+8]$$
$$-(18\gamma-54)\bar{h}'\bar{M}'\bar{M}''\bar{M}-(6\gamma-18)\bar{h}'\bar{M}'^3$$

APPENDIX C

Derivatives of the inverse function used in the computations:

$$\xi = f(\bar{M}) ,$$

so

$$\bar{M}' = (d\xi/d\bar{M})^{-1}$$

$$\bar{M}'' = -\bar{M}'^{3}(d^2\xi/d\bar{M}^2)$$

$$\bar{M}''' = -\bar{M}'^{2}(3\bar{M}'' \cdot d^2\xi/d\bar{M}^2 + \bar{M}'^{2} \cdot d^3\xi/d\bar{M}^3)$$

$$\bar{M}'''' = -3(2\bar{M}'\bar{M}''^{2}+\bar{M}'^{2}\bar{M}''') \cdot d^2\xi/d\bar{M}^2 - 7\bar{M}'^{3}\bar{M}'' \cdot d^3\xi/d\bar{M}^3 - \bar{M}'^{5} \cdot d^4\xi/d\bar{M}^4$$

The derivatives of the chosen centerline distribution are as follows:

$$\xi = \frac{\bar{M}^m - 1}{\bar{M}} \left[\frac{x_t \bar{M}_t}{\bar{M}_t^m - 1} - k(\bar{M}_t - \bar{M})^{1/n} \right] ,$$

so we get

$$\bar{M}\frac{d\xi}{d\bar{M}} + \xi = m\bar{M}^{m-1}\left[\frac{x_t \bar{M}_t}{\bar{M}_t^m - 1} - k(\bar{M}_t - \bar{M})^{\frac{1}{n}} \right] + \frac{k}{n}(\bar{M}^m - 1)(\bar{M}_t - \bar{M})^{\frac{1}{n} - 1} ,$$

$$\bar{M}\frac{d^2\xi}{d\bar{M}^2} + 2\frac{d\xi}{d\bar{M}} = m(m-1)\bar{M}^{m-2}\left[\frac{x_t \bar{M}_t}{\bar{M}_t^m - 1} - k(\bar{M}_t - \bar{M})^{\frac{1}{n}} \right] + \frac{2mk}{n}\bar{M}^{m-1}(\bar{M}_t - \bar{M})^{\frac{1}{n}-1} - \frac{k(1-n)}{n^2}(\bar{M}^m - 1)(\bar{M}_t - \bar{M})^{\frac{1}{n}-2} ,$$

$$\bar{M}\frac{d^3\xi}{d\bar{M}^3} + 3\frac{d^2\xi}{d\bar{M}^2} = m(m-1)(m-2)\bar{M}^{m-3}\left[\frac{x_t\bar{M}_t}{\bar{M}_t^{m-1}} - k(\bar{M}_t-\bar{M})^{\frac{1}{n}}\right]$$

$$+ \frac{3km(m-1)}{n}\bar{M}^{m-2}(\bar{M}_t-\bar{M})^{\frac{1}{n}-1}$$

$$- \frac{3km(1-n)}{n^2}\bar{M}^{m-1}(\bar{M}_t-\bar{M})^{\frac{1}{n}-2}$$

$$+ \frac{k(1-n)(1-2n)}{n^3}\bar{M}^{m-1}(\bar{M}_t-\bar{M})^{\frac{1}{n}-3}$$

and

$$\bar{M}\frac{d^4\xi}{d\bar{M}^4} + 4\frac{d^3\xi}{d\bar{M}^3} = m(m-1)(m-2)(m-3)\bar{M}^{m-4}\left[\frac{x_t\bar{M}_t}{\bar{M}_t^{m-1}} - k(\bar{M}_t-\bar{M})^{\frac{1}{n}}\right]$$

$$+ \frac{4km(m-1)(m-2)}{n}\bar{M}^{m-3}(\bar{M}_t-\bar{M})^{\frac{1}{n}-1}$$

$$- \frac{6km(m-1)(1-n)}{n^2}\bar{M}^{m-2}(\bar{M}_t-\bar{M})^{\frac{1}{n}-2}$$

$$+ \frac{4km(1-n)(1-2n)}{n^3}\bar{M}^{m-1}(\bar{M}_t-\bar{M})^{\frac{1}{n}-3}$$

$$- \frac{k(1-n)(1-2n)(1-3n)}{n^4}\bar{M}^{m-1}(\bar{M}_t-\bar{M})^{\frac{1}{n}-4}$$

APPENDIX D

In Runge-Kutta's method of integration we must integrate

$$\frac{d\theta}{dx} + \theta f(x) = \theta^{-0.268} g(x) \qquad (25)$$

or

$$\theta(x) = \theta(0) + \int_0^x \left[\theta^{-0.268} g(x) - \theta f(x)\right] dx$$

or

$$\theta(x) = \theta(0) + \int_0^x d(\theta, x)dx$$

Taking a discrete number of equal steps (h_n) and considering the fourth order method we get

$$\theta(n+1) - \theta(n) = \frac{1}{6}\left[k_1 + 2k_2 + 2k_3 + k_4\right]$$

where:

$$k_1 = h_n . d(x_n, \theta_n)$$

$$k_2 = h_n . d(x_n + \tfrac{1}{2}h_n, \theta_n + \tfrac{1}{2}k_1)$$

$$k_3 = h_n . d(x_n + \tfrac{1}{2}h_n, \theta_n + \tfrac{1}{2}k_2)$$

$$k_4 = h_n . d(x_n + h_n, \theta_n + k_3)$$